Research Square

Preprints are preliminary reports that have not undergone peer review.
They should not be considered conclusive, used to inform clinical practice,
or referenced by the media as validated information.

The CdGAP C-terminal pro-invasive domain drives breast cancer metastasis and activates WNT signaling

Nathalie Lamarche-Vane

nathalie.lamarche@mcgill.ca

Research Institute of McGill University Health Centre https://orcid.org/0000-0002-9540-3157

Monica Lara-Marquez

Nadia Boufaied

YI HE

McGill University/RI-MUHC

Jennifer Chapelle

Jalal Al Rahbani

Ellie Massey

Nadia Azougagh

Alex Gregorieff

David Labbé

McGill University https://orcid.org/0000-0001-8864-8765

Article

Keywords:

Posted Date: June 26th, 2026

DOI: https://doi.org/10.21203/rs.3.rs-9917734/v1

License: This work is licensed under a Creative Commons Attribution 4.0 International License.
Read Full License

Additional Declarations:
There is **NO** conflict of interest to disclose.

Table 1 to 6 are available in the Supplementary Files section.

The CdGAP C-terminal pro-invasive domain drives breast cancer metastasis and activates WNT signaling

Mónica Lara-Márquez[1,2], Nadia Boufaied[1*], Yi He[1,2,*], Jennifer Chapelle[1,2], Jalal Al Rahbani[1,2], Ellie J. Massey[1], Nadia Azougagh[1], Alex Gregorieff[1,2,3], David P. Labbé[1,2,4,‡], Nathalie Lamarche-Vane[1,2,‡]

[1]Cancer Research Program, Research Institute of the McGill University Health Centre, Montréal, QC H4A 3J1, Canada

[2]Department of Anatomy and Cell Biology, McGill University, Montréal, QC H3A 0C7, Canada

[3]Department of Pathology, McGill University, Montréal, QC H3A 0C7, Canada

[4]Division of Urology, Department of Surgery, McGill University, Montréal, QC H4A 3J1, Canada

[*]These authors contributed equally to this work

[‡]Corresponding authors

Correspondence: Dr. David P. Labbé, McGill University, Research Institute of the McGill University Health Centre, 1001 Decarie Boulevard, E02.6217, Montréal, Québec H4A 3J1, Canada. Phone: 514-934-1934 ext.76361, Fax: 514-933-2691, E-mail: david.labbe@mcgill.ca; Dr. Nathalie Lamarche-Vane, McGill University, Research Institute of the McGill University Health Centre, 1001 Decarie Boulevard, E02.6230, Montréal, Québec H4A 3J1, Canada. Phone: 514-934-1934 ext 76166,Email: nathalie.lamarche@mcgill.ca.

Authors' Disclosures

The authors declare no financial and/or non-financial competing interests.

Abstract

Triple-negative breast cancer (TNBC) is an aggressive disease with limited therapeutic options and a high propensity for metastasis. Cdc42 GTPase-activating protein (CdGAP/ARHGAP31) is highly expressed in TNBC, yet the molecular determinants underlying its pro-metastatic activity remain unclear. Here, we identify a pro-invasive domain (PID) within the C-terminus of CdGAP required for breast cancer progression and metastasis. Using an $HER2^{+}$ mouse mammary tumor model and genetic knock-out and knock-in models in TNBC cells, we show that loss of CdGAP C-terminus suppresses tumor cell proliferation, migration, invasion, and lung metastasis without affecting primary tumor formation. Mechanistically, CdGAP PID interacts with the LIM-domain protein LIMD1 at focal adhesions to regulate cell morphology and adhesion dynamics. Transcriptomic profiling reveals that CdGAP and its C-terminal PID control a shared gene expression program enriched for WNT signaling. Accordingly, deletion of CdGAP C-terminus impairs canonical WNT/β-catenin signaling by increasing expression of the WNT inhibitor KREMEN1 and reducing LRP6 cell-surface availability. Importantly, a CdGAP-associated WNT transcriptional signature predicts reduced metastasis-free and overall survival in TNBC patients. Collectively, these findings uncover a GAP-independent, pro-invasive function of CdGAP that links focal adhesion dynamics to WNT pathway activation, highlighting the CdGAP C-terminus as a potential therapeutic target in aggressive breast cancer.

Introduction

Breast cancer is a heterogeneous disease and the most commonly diagnosed cancer among women worldwide [1]. Metastatic dissemination is the leading cause of breast cancer-related mortality. Among the molecular subtypes of breast cancer, amplification of the human epidermal growth factor receptor 2 (HER2/NEU) occurs in approximately 15% of primary breast tumors and is associated with early metastatic progression and poor survival rates when developing resistance to anti-HER2 therapies. In contrast, triple negative breast cancer (TNBC), defined by the absence of estrogen receptor (ER), progesterone receptor (PR), and HER2 expression, accounts for 15-20% of all breast cancers [2]. TNBC is highly invasive and is associated with shorter patient survival due to its increased propensity for distant metastasis, particularly to the brain and visceral organs, as well as the lack of effective targeted therapies. Given the central role of metastatic dissemination in breast cancer mortality, there is a pressing need to identify the molecular regulators that promote invasive and metastatic behavior. In this context, defining the signaling pathways that regulate cell migration, adhesion, and metastatic progression is essential for the development of new therapeutic strategies.

Rho GTPases act as molecular switches to regulate gene expression, cytoskeletal dynamics, and the cell cycle. They are positively regulated by guanine nucleotide exchange factors (GEFs) and negatively by GTPase-activating proteins (GAPs) and guanine nucleotide dissociation inhibitors (GDIs) [3]. Even though numerous RhoGAPs have been described as tumor suppressors due to their ability to inactivate Rho GTPases, new evidence identifies some of them as oncoproteins [4]. Cdc42 GTPase-activating protein (CdGAP, also known as ARHGAP31), is a RhoGAP for the GTPases Rac1 and Cdc42 [5]. CdGAP has been previously established as a positive modulator of HER2-positive (HER2+) breast cancer and prostate tumor progression and

metastasis [6-8]. The crosstalk of CdGAP with the tumor suppressor protein deleted in colorectal cancer 1 (Dlc1)-RhoA axis and the modulation of TGF-β-mediated cellular processes facilitate cell proliferation, migration, invasion, and metastasis in HER2+ breast cancer [7]. Additionally, the proline-rich domain (PRD) of CdGAP mediates the transcriptional co-repression of E-cadherin, promoting epithelial-to-mesenchymal transition [6]. Of interest, the loss of the PRD and C-terminal region in CdGAP due to premature termination mutations in patients with the rare developmental Adams-Oliver Syndrome (AOS) results in phenotypic cellular changes involving aberrant GAP activity, cell migration and proliferation, in addition to the lack of E-cadherin repressing activity [9, 10]. Thus, these previous studies underscore the importance of the C-terminus in CdGAP cellular functions, which presents notable features because it encompasses GAP-independent functions including protein-protein interactions, post-translational modifications, and transcriptional activities that could potentially enable cancer cells to adopt aberrant phenotypes. However, how the C-terminus region of CdGAP contributes to breast tumorigenesis and progression remains unknown.

In this study, we explored the contribution of the CdGAP C-terminus to key cellular processes involved in tumor progression and metastasis. We identified the CdGAP C-terminus as a pro-invasive domain (PID) required to promote breast cancer metastasis to the lungs in a HER2+ murine breast cancer model. In addition, the CdGAP C-terminus modulated cell morphology, cell-cell adhesion, proliferation, migration, invasion, and metastatic potential in TNBC. We further identified a novel interface between the CdGAP C-terminus and LIMD1 at focal adhesions in TNBC cells, where these proteins cooperatively controlled cytoskeletal rearrangements and focal adhesion dynamics. Furthermore, we demonstrated that the CdGAP C-terminal region mediated crosstalk with the activation of the canonical WNT/β-catenin signaling pathway. It significantly

89 impacted a WNT signaling gene signature in TNBC that is associated with poor overall survival
90 in patients. Collectively, these findings establish CdGAP C-terminus as a novel therapeutic target
91 in the most aggressive breast cancer molecular subtypes and support new opportunities for
92 targeting WNT signaling pathway in TNBC.

Materials/Subjects and Methods

In vivo mouse model

Transgenic *Mouse Mammary Tumor Virus (MMTV)*-Neu FVB/NJ (MMTV-NeuNDL2-5) mice was previously described [11]. The *CdGAP (P668T P670X)* knock in (ki) mice were generated by McGill Integrated Core for Animal Modeling. CRISPR/Cas9 technology was used to generate the *CdGAP P668T P670X* allele (Supplementary Fig. 1A), which encodes the truncated mutant form of CdGAP lacking the C-terminal end of this protein. For targeting *CdGAP P668T P670X*, three Guide RNAs (gRNAs) (Supplementary Table 1) were designed following the instructions at http://crispr.mit.edu/. Mice were generated by electroporation of the three gRNAs and Cas9 protein into single-cell FVB/NJ mouse zygotes. Live pups born from these females were genotyped by PCR amplification of genomic DNA extracted from the tail. The targeted region was amplified using the genotyping primers (5'CAGCCATGGTTACTGAGGC3'; 5'AGTAAGAGGGGGAGAGAGATTCC3') (Supplementary Table 2). The products were sent for direct Sanger sequencing (Génome Québec). Instead of 5' **CCG**ATT**CCT** 3' in wild-type *CdGAP* sequence, two founder males had established 5'**ACG**ATT**TAA** 3' mutations in their two *CdGAP* alleles. Founder mutants underwent at least 2 generations of backcrossing with wild-type FVB/N mice before establishing progeny. Heterozygous $CdGAP^{wt/ki}$ mice were intercrossed to generate $CdGAP^{wt/wt}$, heterozygous $CdGAP^{wt/ki}$, and homozygous $CdGAP^{ki/ki}$ animals. After producing 10 generations of progeny from the mating of heterozygous mice, backcrossing was performed with wild-type FVB/NJ (Charles River) mice before continuing with further analysis. All tail veins experiments were performed in 8-weeks female athymic mice purchased from Charles River Laboratories. All animal protocols (protocol no. 7665) were approved by McGill

University Animal Use and Care Committee, in accordance with guidelines established by the Canadian Council on Animal Care.

Whole-Mount analysis of mammary glands

CdGAP$^{ki/ki}$ mice were intercrossed with FVB/NJ mice to determine if mammary gland development requires the C-terminal region of CdGAP. The #4 and #9 mammary glands were collected from 9-, 12-, and 15-weeks old *CdGAP*$^{wt/wt}$ or *CdGAP*$^{ki/ki}$ mice. Mammary glands were stained in carmine red solution, dehydrated in an ethanol gradient, cleared in xylene, and mounted using Permount (Fisher). The developmental status of the mammary gland was determined by counting the mammary tree branching from the nipple to the last branch. Quantification of Mammary Intraepithelial Neoplastic (MIN) lesions was done in the same way on tumor-free mammary glands #4 and #9 from *Neu*$^{+}$*CdGAP*$^{wt/wt}$ and *Neu*$^{+}$*CdGAP*$^{ki/ki}$ mice at 5 weeks after tumor onset [12]. The total amount of MIN lesions was counted under the microscope.

Tumor progression studies

CdGAP$^{ki/ki}$ mice were intercrossed with *MMTV-Neu* transgenic mice to generate large cohorts of female mice. The mammary tumor formation was determined by manual palpation weekly. Each female mouse was euthanized 5-weeks after tumor onset and analyzed by collecting the mammary glands, tumors, and lungs. The amount and volume of tumor nodules and the presence of lung lesions were determined as previously described [12]. The lungs were embedded in paraffin and cut at 4 µm every 100 µm followed by staining with hematoxylin and eosin (H&E). Lung metastatic lesions were counted under the microscope.

Intravasation Assay

The quantification of Circulating Tumor Cells (CTCs) was performed as previously described [6]**.** After 5-weeks tumor onset, 0.5-1ml of the circulating blood was drawn by cardiac puncture from

anesthetized *Neu*$^{+}$*CdGAP*$^{wt/wt}$ and *Neu*$^{+}$*CdGAP*$^{ki/ki}$ female mice. Blood was plated directly in DMEM (Wisent: 319-005-CL) with 5% fetal bovine serum (FBS), 150 µl of 10 mM EDTA and 1x Mammary Epithelial Growth Supplement (MEGS) (ThermoFisher: S0155). Media was gently changed to remove the red blood cells without disturbing the attached tumor cells once every three days. After 14 days, tumor cell colonies were counted. Tumor blood burden was calculated as the total colonies divided by the volume of blood taken and tumor weight collected.

Public clinical data analysis

Cancer type and clinical characteristics associated with CdGAP genomic and transcriptomic alterations were evaluated using the Molecular Taxonomy of Breast Cancer International Consortium (METABRIC) dataset (n=1866) [13, 14] and cBioPortal platform for cancer genomics [15-17]. CdGAP expression in breast cancer cell lines was analyzed using the Broad Institute DepMap Expression Public 23Q4 dataset, which includes 66 breast cancer cell lines (data available at https://depmap.org). Survival analyses were performed using three publicly available breast cancer cohorts. Data from the Jézéquel cohort (GSE58812) [18] and Brueffer cohort (GSE96058) [19] were obtained from the Gene Expression Omnibus (GEO), whereas data from the Metastatic Breast Cancer (MBC) project [20] were retrieved through cBioPortal (https://www.cbioportal.org/study/summary?id=brca_mbcproject_wagle_2017). Only patients with TNBC, as defined in the original studies and with available survival data, were included in these analyses.

Cell lines and treatment

MDA-MB-231 (ATCC HTB-26, RRID: CVCL_0062), HS578T (ATCC HTB-126, RRID: CVCL_0332), and HEK293 (ATCC, CRL-1573, RRID: CVCL_0045) cells were cultured in DMEM (Wisent: 319-005-CL) supplemented with 10% fetal bovine serum (FBS) (Wisent:

090150), 1% penicillin/streptomycin (Wisent: 450-201-EL) and maintained in a 5% CO2 atmosphere at 37°C. The cell lines were routinely tested for the presence of mycoplasma contamination using the mycoplasma PCR detection kit (ZmTech: M209001). Cell lines authentication was done using Short Tandem Repeat (STR) analysis (GeneCopoeia). For stimulation of the Wnt signaling pathway, MDA-MB-231 cells were treated for 24 hours with 5% conditioned medium (CM) derived from an L cell line engineered to secrete Wnt3a, R spondin 3 and Noggin (L-WRN) [21].

Transfection and plasmids

Transfections of TNBC cell lines were performed using the JetPrime in vitro DNA & siRNA transfection kit (Polyplus: 101000046) at a ratio 1:2 (DNA: reagent) following the guidelines provided. HEK293 cells were transfected with the indicated plasmids with polyethyleneimine (PEI; PolySciences, PA). The plasmid and PEI reagent were mixed at a ratio 1:2.5 (DNA: PEI) as described before [6]. A list of plasmids used for cell transfections is shown in Supplementary Table 3 [22-24].

Generation of CdGAP knock-out (KO), LIMD1 KO, and CdGAP knock-in (KI) monoclonal cell lines by CRISPR/Cas9

LIMD1 KO, CdGAP KO and KI cell lines were generated using the CRISPR/Cas9 technology [25]. Using the online tool Benchling (https://benchling.com), the 20 nucleotide-single guide RNAs (sgRNAs) were designed (Supplementary Table 1) and subcloned into the pSpCas9(BB)-2A-Puro (Px459) V2.0 plasmid system. The oligonucleotide primer pairs were 5' phosphorylated by incubating them with T4 polynucleotide kinase (New England BioLabs: M0201S) in T4 DNA ligase Reaction Buffer (New England BioLabs: B0202S) for 30 min at 37°C. Next, oligonucleotides were incubated in a 95°C heat block for 5 min, followed by removing the block

184 from the heat and allowed to cool down to 25°C. The annealed oligonucleotides were diluted 1:200
185 in sterile water. The Px459 plasmid was digested with FastDigest Bpil in 10X FastDigest Buffer
186 (Thermo Scientific: FD1014) for 1h at 37°C, followed by dephosphorylation using FastAP
187 thermosensitive alkaline phosphatase (Thermo Scientific: EF0654) for 30 min at 37°C. The
188 phosphorylated oligonucleotides were ligated with the digested Px459 plasmid using T4 DNA
189 ligase in T4 DNA ligase Reaction Buffer at 16 °C overnight. Plasmids were transformed into
190 DH5α competent cells (Invitrogen: 18258-012) and isolated using the PureLink™ HiPure Plasmid
191 Maxiprep kit (Invitrogen: K210007). TNBC cell lines were transfected with plasmids as described
192 above and cells were selected with puromycin (1 μg/ml) (Sigma-Aldrich: G9023) 72h post-
193 transfection. To isolate clonal cell lines, cells were serially diluted in 96-well plates. After clonal
194 expansion, detection of CdGAP or LIMD1-depleted and CdGAP KI cell lines were assessed by
195 immunoblotting. Due to the inherent variability of the non-homologous end joining (NHEJ) repair
196 pathway, resulting CdGAP KI proteins displayed differences in molecular weight due to variable
197 frameshift length. Genomic DNA was extracted from monoclonal cell lines, and the targeted
198 region was amplified by PCR and submitted for Sanger sequencing. Open reading frames (ORFs)
199 were analyzed using the online ORF finder tool https://www.ncbi.nlm.nih.gov/orffinder/, and the
200 presence or absence of stop codons was manually verified by scanning for in-frame TAA, TAG,
201 or TGA codons. The two monoclonal cell lines derived from parental HS578T were identical,
202 expressing a truncated version of CdGAP corresponding to amino acids 1–681 followed by a
203 frameshift extension to residue 692. From parental MDA-MB-231 cells, KI1 cell lines expressed
204 a variant consisting of residues 1–680 followed by a frameshift extension to residue 768, while
205 KI2 expressed a 1–680 variant with a longer frameshift extension, explaining the increased

molecular weight. Despite these frameshift differences, all KI variants served as functional models to study the role of the C-terminal region of CdGAP.

Immunoprecipitation and immunoblotting

As described previously [7], cells were lysed in RIPA buffer (50 mM HEPES pH 7.5, 0.1% sodium dodecyl sulfate, 1% Triton X-100, 0.5% sodium deoxycholate, 50 mM sodium fluoride, 150 mM sodium chloride, 10 mM EDTA pH 8.0, 50 mM sodium orthovanadate, 20 mM leupeptin, 20 mM aprotinin and 1 mM phenylmethylsulphonyl fluoride). Next, the protein lysates were subjected to centrifugation at 10,000 × g for 15 min at 4 °C to remove insoluble materials. Sample protein concentration was determined using the Bicinchoninic Acid Assay (BCA) protein kit (Thermo-Scientific: 23225). Protein samples were resolved by sodium dodecyl sulfate-polyacrylamide gel electrophoresis (SDS-PAGE), transferred to nitrocellulose membranes, and immunoblotted with the indicated antibodies in Supplementary Table 4. Finally, membranes were visualized by enhanced chemiluminescence (ECL) using Clarity™ western ECL substrate (Bio-Rad: 1705061) and the ChemiDoc™ MP imaging system. Quantitative densitometry analysis was carried out using Image Lab software 6.0.1 (RRID: SCR_014210). For the immunoprecipitation experiments, samples were lysed, cleared, and quantified as described above. Next, lysates were pre-cleared by incubating 1.5 mg of protein extracts with Protein G Sepharose™ 4 Fast Flow beads (Cytiva: 17061801) and rabbit IgG antibody for 1h in constant rotation at 4 °C. Next, samples were incubated with the indicated antibody overnight followed by incubation with beads for 2h. Beads were washed with lysis buffer and heated to 95°C in SDS sample buffer. Protein samples were resolved by SDS-PAGE, transferred to nitrocellulose membranes for immunoblotting.

Rac1 activation G-LISA assay

Levels of GTP-bound Rac1 were measured using a luminescence-based G-LISA™ Rac1 activation assay Biochem kit™ (Cytoskeleton: BK126) according to the manufacturer's protocol. Briefly, cells were cultured overnight in p60 plates (3.5 x10^5 cells/plate). Next, cells were lysed, and equal amount of protein lysates were incubated in the Rac-GTP binding 96-well plate provided. Subsequently, samples were incubated with Rac1 primary antibody, followed by an HRP-conjugated secondary antibody. Luminescence was determined using a Tecan infinite M200 pro microplate reader. Constitutively active Rac1 protein provided by the manufacturer were used as positive control.

Immunofluorescence

Cells were cultured (4.5x10^4 cells/well) on fibronectin-coated coverslips in 24-well plates and incubated overnight. Cells were fixed with 4% paraformaldehyde, washed twice with PBS followed by permeabilization with 0.25% Triton-X-100. Next, cells were washed with PBS and incubated with blocking buffer 0.5% bovine serum albumin (BSA). Actin staining was done with phalloidin-TRITC (Sigma-Aldrich: P1951, RRID: AB_2315148), and DAPI for 45 min at RT in 0.1% BSA. Antibodies used for immunofluorescence are shown in Supplementary Table 4. Images were taken using a ZEISS LSM 780 laser scanning confocal microscope with a Plan-Apochromat 20x/0.8 M27 objective lens and a PLAN-Neofluar40x/1.4 oil corr LD objective lens. Cell morphology analysis was done using the Fiji-Image J software, version 1.8.0/1.53a (RRID: SCR_ 003070).

Cell proliferation assay

Cell growth was assessed by cell number quantification using trypan blue staining as previously described [26]. Cells were seeded (3x10^3 cells/well) in 96-well plates. Next, cells were serum-starved overnight for synchronisation followed by stimulation with 10% serum containing medium

for 72h. Cells were collected by trypsin detachment, cell suspension was mixed 1:1 with 0.4% trypan blue solution (Sigma-Aldrich: T8154) and the number of total and viable cells was determined by manual quantification.

3D culture assay and immunostaining

As described previously [7], in 8-well chamber plates pre-coated with 40 µl of Corning™ Matrigel™ GFR membrane matrix (Thermo Fisher Scientific: CB-40230A), MDA-MB-231 cell lines were seeded ($2X10^3$ cells per well) in 400 µl of 2% Matrigel in supplemented DMEM. Fresh media was replaced after 4 days of culture. To observe the spheroids by immunofluorescence, samples were fixed in methanol: acetone 1:1 at -20 °C for 10 min. Next, using blocking buffer (0.1% BSA, 0.2% Triton X-100, 0.05% Tween-20, 10% goat serum (Sigma: G9023) in PBS) spheroids were incubated overnight at room temperature. Phalloidin-TRITC and DAPI were used to stain F-actin and DNA, respectively. Z-stack Images were taken using a Zeiss LSM780 laser-scanning confocal microscope with a Plan-Apochromat20x/0.8 M27 LD objective lens. Spheroid relative area and convex area were measured using the Fiji-Image J Software.

Dual Luciferase assay (DLR)

To determine TCF/LEF transcriptional activity, TNBC cell lines were co-transfected with M50 Super 8x TOPFlash plasmid (a gift from Randall Moon (Addgene plasmid #12456)) and the pGL4 renilla luciferase reporter plasmid. Four hours post-transfection, cells were treated with 5% L-WRN CM or control media for 24h, followed by the luciferase assays using the Dual Luciferase Assay kit (Promega: E1910) as described previously [6].

Wound healing scratch assay

Cells were cultured to 80-90% confluency in 96-well Image Lock microplates (Sartorius: 4379) coated with poly-D-lysine hydrobromide (Sigma-Aldrich: P6407) and incubate overnight. The Woundmaker™ (Essen Bioscience) was used to create homogeneous wounds. Phase contrast pictures were taken every 2-3 hours and analyzed with IncuCyte Zoom Live Cell Imaging microscope and software (Essen BioScience) for 24 h.

Migration and invasion transwell assays

For migration assays of TNBC cell lines, $3.5x10^4$ cells were resuspended in serum-free DMEM and seeded in the top chamber of transwell inserts (Falcon: 353097). For invasion assays, $5x10^4$ cells were plated onto transwell inserts coated with 5% Corning™ Matrigel™ membrane matrix (Thermo Fisher Scientific: CB-40234A). Cells were incubated at 37 °C overnight to allow cell motility towards the bottom chamber containing DMEM supplemented with 10% FBS. Cells on the bottom surface of the insert were fixed in 10% formalin (BioShop: 8G56294) and stained with a crystal violet solution. Images were taken for each transwell insert using a Nikon inverted microscope camera with a 10× objective lens (Nikon Eclipse TE300 Inverted microscope). Quantitative analysis was assessed using Fiji-Image J software. Data represented the fold change of cells migrated relative to control cells obtained from at least three independent experiments.

Tail vein injection and immunohistochemistry

We performed tail vein injections in athymic female mice with MDA-MB-231 CdGAP mutant cell lines ($1x10^6$ cells in 100 µl of PBS per mice) as previously reported[27]. After 5 weeks, lungs were collected, fixed in 10% formalin and paraffin embedded. Samples were cut at 4 µm every 100 µm and stained with haematoxylin and Eosin. Slides were scanned using a Scanscope XT digital slide scanner (Aperio, Leica Biosystems Inc.). The area of the metastatic lesions was compared to the

total lung area analyzed by Imagescope software (Version 2.0.0, Aperio, Leica Biosystems Inc.). For *Neu*$^{+}$*CdGAP*$^{wt/wt}$ and *Neu*$^{+}$*CdGAP*$^{ki/ki}$ tumor analysis, tumors were fixed in 10% formalin and paraffin embedded. Antibodies used for IHC are listed in Supplementary Table S4.

Real time quantitative PCR (RT-qPCR)

Evaluation of gene transcriptional expression was done as described before [7]. Briefly, RNA was extracted using the RNeasy Mini Kit (Qiagen: 74104). The iScript^{TM} Reverse Transcription Supermix (Bio-rad: 1708841) was used to generate cDNA from 2 μg of total RNA. qPCR was performed using the SsoAdvancedTM Universal SYRB ® Green Supermix (Bio-rad: 1725271) with the primers listed in Supplementary Table 3. Gene expression was normalized to β-actin RNA expression.

RNA-sequencing and data processing

RNA-seq was performed as previously described [6]. Total RNA was extracted from MDA-MB-231 CdGAP KO1 and KI1 cell lines in triplicate using the RNeasy Mini Kit and purified with RNase-free DNase set (Qiagen: 79254). Deep sequencing was performed using Illumina TruSeq RNA Sample Preparation Kit, Illumina TruSeq SR Cluster Kit v2, and Illumina TruSeq SBS Kit v2 (50 cycles) according to the manufacturer's procedures. RNA-seq alignment was performed using GenPipes "RNAseq" pipeline[28]. Raw reads were trimmed and filtered for quality using Trimmomatic [29] and then mapped to the human reference genome (*Homo sapiens* GRCh38) by STAR [30]. Mapped reads were further refined using GATK [31] and Picard suite (http://broadinstitute.github.io/picard/) and gene level count was quantified using HT-seq [32]. R software (v. 4.1.1, R-project.org) and a customized R-script were used for downstream analysis. Differentially expressed genes were identified using the DESeq2_1.32.0 package[33]. Genes were considered differentially expressed if the log (fold change) was higher than 1 with a p-value < 0.05

and an adjusted p-value < 0.05. ClusterProfiler package_4.0.5 [34, 35] was used to run the gene ontology (GO) term analysis and Gene set enrichment analysis (GSEA) using the Hallmark Molecular Signature Database (H, v.5; MSigDB) [36].

LRP6 surface staining

MDA-MB-231 cells were cultured in 60 mm plates at 50% confluency and allowed to attach overnight. Cells were treated with 5% L-WRN CM for 24 h. For LRP6 staining, a modified protocol from [37] was used. Briefly, cells were detached and washed twice with FACS buffer (2% FBS, EDTA 2mM in PBS). Cell suspension was adjusted to 1 million cells/ml and blocked with 10% FBS in FACS buffer for 30 min on ice, followed by staining with LRP6 antibody or mouse gamma globulin as Isotype control for 30 min on ice. After two washes, secondary antibody coupled to Alexa Fluor 647 staining for 30 min on ice was performed. Samples were washed, stained with DAPI and up to 10 000 events of live cells per condition were recorded and analyzed by flow cytometry with a BD FACSCanto II.

Survival analysis

RNA-seq expression data were normalized for sequencing depth and transformed to TPM (transcripts per million), whereas microarray gene expression data were RMA-normalized and log-transformed. These normalized datasets were then used to generate a WNT signature score based on the 18 genes identified by GO biological process overrepresentation analysis using the singscore_1.22.0 package [38]. Kaplan-Meier analysis and log-rank tests were used to compare metastasis-free survival and overall survival between patients with high and low CdGAP-dependent WNT signature scores. The signature score threshold was determined using cutpointr_1.2.0 package [39], and survival analyses were performed using survival_3.8-3 [40] and survminer_0.5.0 packages [41].

Statistical analysis

Statistical analysis was done using GraphPad Prims 10.2.0. The significance of the difference among groups was evaluated by ordinary one-way ANOVA with Tukey's multiple comparisons test. The wound healing scratch assays were analyzed with multiple unpaired t tests with the Two-stage step-up method (Benjamini, Krieger, and Yekutieli). Data are presented as the mean ± standard error of mean (SEM), and p value less than 0.05 was considered statistically significant**.**

Data availability

GEO accession number for RNA-seq data is GSE327407.

Results

The CdGAP C-terminus promotes metastatic progression in HER2^{+} breast cancer

Given the established pro-metastatic role of CdGAP in HER2+ breast cancer [7], we asked whether its C-terminus is required for tumor progression and metastatic dissemination *in vivo*. To examine the function of the C-terminus *in vivo*, we generated a *CdGAP (P668T P670X)* knock-in (ki) mouse model corresponding to the human *CDGAP-Q683X* AOS variant [9] using a CRISPR/Cas9 strategy (Supplementary Fig. 1A). We first found that deletion of the CdGAP C-terminus did not affect the mammary gland development. Similar to the complete loss of CdGAP in the mammary gland [7], we observed no significant difference in ductal branching between control *CdGAP$^{wt/wt}$* and *CdGAP$^{ki/ki}$* mice at 9, 12, and 15 weeks (Supplementary Fig. 1B). Next, we intercrossed *CdGAP$^{ki/ki}$* with mouse mammary tumor virus *(MMTV)-Neu* mice [11] to assess tumor progression in females (Fig. 1A). In this mouse model, an activated form of Neu (NeuNDL2-5) is expressed in the mammary gland of mice using the MMTV promoter, which results in tumors that progress to invasive carcinoma and lung metastasis [11]. Three cohorts of mice (Neu^{+}CdGAP$^{wt/wt}$; Neu^{+}CdGAP$^{ki/wt}$; Neu^{+}CdGAP$^{ki/ki}$) were generated and monitored for tumor growth. Tumors were collected and analyzed 5 weeks after onset. The CdGAP ki allele was confirmed (Fig. 1B) and the truncated CdGAP protein lacking the C-terminus was detected in mammary tumor protein lysates (Fig. 1C). We found that deletion of the C-terminus caused a modest delay in tumor onset for Neu^{+}CdGAP$^{ki/ki}$ compared to Neu^{+} control, whereas there was no delay for Neu^{+}CdGAP$^{ki/wt}$ (Fig. 1D). To characterize the tumor initiation process, we quantified the number of mammary intraepithelial neoplastic (MIN) lesions on inguinal mammary gland and we observed no difference between Neu^{+}CdGAP$^{ki/ki}$ and Neu^{+} control mice, suggesting that neoplastic initiation occurs normally in the absence of the C-terminus (Fig. 1E). Furthermore, all

genotypes showed a similar tumor mass (Fig. 1F), primary tumor number (Fig. 1G), and solid adenocarcinoma histology (Supplementary Fig. 1C), indicating that the loss of the C-terminus did not affect tumor formation or differentiation state. No difference in staining by markers of cell proliferation (Ki-67), angiogenesis (CD31), and cell apoptosis (cleaved caspase 3) was observed between $Neu^{+}CdGAP^{ki/ki}$ and Neu^{+} control mice (Supplementary Fig. 1D-F). Strikingly, although $Neu^{+}CdGAP^{ki/ki}$ and $Neu^{+}CdGAP^{wt/wt}$ mice developed histologically similar adenocarcinoma metastatic lesions (Fig. 1H), both the frequency and number of lung metastases were significantly reduced in $Neu^{+}CdGAP^{ki/ki}$ and $Neu^{+}CdGAP^{ki/wt}$ mice compared with controls (Fig. 1I, J). Because we have previously shown that CdGAP is required at multiple steps of HER2+-driven metastasis [7], we next determined whether the C-terminus was also required to promote breast tumor cell intravasation *in vivo*. We quantified circulating tumor cells (CTCs) when primary tumors had reached a tumor volume of 1.5 cm^3 and found that $Neu^{+}CdGAP^{ki/ki}$ mice presented a significant reduction in CTCs compared to control mice (Fig. 1K). Altogether, these data demonstrate that the CdGAP C-terminus is essential for promoting HER2+ breast cancer metastasis.

The CdGAP C-terminus regulates proliferation and morphology in TNBC cells

To further define the contribution of the CdGAP C-terminus to breast cancer progression, we first examined the clinical relevance of CdGAP across breast cancer molecular subtypes using the publicly available METABRIC dataset [13, 14] and cBioPortal [15-17]. We found that *CdGAP* genetic alterations were most prevalent in ER-/HER2- tumors (n=1667; $p < 10^{-10}$) (Supplementary Fig. 2A) and in PR-negative tumors (n=1866; $p=2.22X10^{-8}$) (Supplementary Fig. 2B), and were significantly enriched in basal-like and Claudin-low subtypes (n=1866; $p < 10^{-10}$) (Supplementary Fig. 2C). Most *CdGAP* alterations corresponded to changes in CdGAP mRNA expression (Supplementary Fig. 2D) and were more frequent in histological grade 3 tumors ($p=4.6X10^{-3}$)

(Supplementary Fig. 2E). Consistent with these observations, TNBC-derived breast cancer cell lines expressed higher levels of CdGAP mRNA than ER+ and HER2+ cell lines (Fig. 2A). Together, these findings identify TNBC as a clinically relevant context in which *CdGAP* is dysregulated and support potential oncogenic role for CdGAP in this subtype. We therefore investigated the functional role of the CdGAP C-terminus in TNBC cells by generating monoclonal cell lines lacking CdGAP or expressing a C-terminally truncated CdGAP mutant using CRISPR/Cas9. We targeted exons 1 and 12 to delete CdGAP in TNBC cell lines. To remove the C-terminus of CdGAP (CdGAP knock-in (KI)), we introduced a premature termination codon in exon 12 to mimic the truncating CdGAP AOS mutation p.Gln683X (Fig. 2B) [9, 42]. We generated MDA-MB-231 and HS578T cell lines depleted of CdGAP expression (CdGAP KO1 and KO2) or expressing CdGAP lacking the C-terminus (~95 kDa band, CdGAP KI1 and KI2) (Fig. 2B).

Although CdGAP negatively regulates Cdc42 and Rac1 through its GAP activity[5], overall levels of active Rac1 remained unchanged in CdGAP KO and KI MDA-MB-231 cells compared with control cells (Supplementary Fig. 3A), suggesting that CdGAP depletion or C-terminal truncation is not sufficient to alter global Rac1 activity in these cells. We next determined the proliferative response of CdGAP mutant TNBC cell lines. CdGAP KO and KI MDA-MB-231 and HS578T cells showed a significantly reduced proliferative capacity over 3 days (Supplementary Fig. 3B, C), indicating that the CdGAP C-terminus is required for the regulation of TNBC cell proliferation. Because actin cytoskeletal remodeling is essential for the formation of protrusive structures at the leading edge and retraction at the rear end during migration [43], we next examined the effects of CdGAP loss or C-terminal truncation on TNBC cell morphology. CdGAP-depleted MDA-MB-231 (Fig. 2C, D) and HS578T cells (Supplementary Fig. 3D, E) displayed increased cell area relative to controls, consistent with a shift toward a more epithelial-

like morphology. In CdGAP KI MDA-MB-231 cells, cell area was also increased (Fig. 2C, D) whereas CdGAP KI HS578T cells showed reduced cell area compared with controls (Supplementary Fig. 3D and E). Despite these differences, both models exhibited a more elongated morphology than control and CdGAP KO cells (Fig. 2C, E; Supplementary 3D and F). Overall, these results indicate that the loss of CdGAP and truncation of its C-terminal region alter TNBC cell morphogenesis, resulting in distinct morphological phenotypes.

CdGAP modulates TNBC cell-cell adhesion, migration, invasion, and lung metastatic potential through its C-terminal region

Because loss of CdGAP or truncation of its C-terminus altered TNBC cell morphology, we next asked whether these changes were accompanied by defects in cell-cell adhesion and invasive behavior. Previous studies showed that reduced CdGAP expression restores and stabilizes cell-cell junctions in normal epithelial cells and in HER2+ breast cancer cells [6, 44]. We therefore used a 3D Matrigel spheroid assay to assess how CdGAP loss or C-terminal truncation affects multicellular organization and invasive growth in TNBC cells. CdGAP KO and KI MDA-MB-231 spheroids displayed a significant reduced relative area after 8 days in culture compared with control spheroids (Fig. 2F, G). Furthermore, solidity analysis (area/convex area) revealed that CdGAP KO and KI spheroids adopted a more compact and well-defined morphology than control spheroids (Fig. 2F, H), consistent with strengthened cell-cell adhesion and reduced invasive architecture.

We next tested whether these structural changes were associated with impaired migratory and invasive behavior. In wound-healing assays, CdGAP-depleted and CdGAP KI cells showed impaired cell migration in both MDA-MB-231 (Fig. 3A and Supplementary Fig. 4A, B) and HS578T cells (Fig. 3B and Supplementary Fig. 4C, D). Likewise, transwell migration assays

showed that CdGAP depletion or expression of the C-terminally truncated CdGAP-KI mutant significantly decreased chemotactic migration and invasion in both MDA-MB-231 (Fig. 3C**,** D and Supplementary Fig. 4E) and HS578T cells (Fig. 3E, F and Supplementary Fig. 4F). Re-expression of myc-tagged CdGAP restored cell migration in CdGAP KO1 MDA-MB-231 cells (Fig. 3 G-I), supporting a specific role for CdGAP in this phenotype. Finally, because CdGAP and its C-terminus promote HER2+ breast cancer metastasis *in vivo* (Fig. 1) [7], and because CdGAP-deficient TNBC cells displayed impaired migration and invasion in vitro, we asked whether these defects translated into reduced lung colonization *in vivo* (Fig. 3J). Consistent with this idea mice injected with CdGAP-depleted or CdGAP KI MDA-MB-231 cells developed fewer lung metastatic lesions than control mice (Fig. 3K and Supplementary Fig. 5). Collectively, these findings indicate that the CdGAP C-terminus is required to sustain the invasive and metastatic behavior of TNBC cells.

The CdGAP C-terminus interacts with the LIM domain-containing protein LIMD1

Because the CdGAP C-terminus was required for TNBC cell migration, invasion and metastatic potential, we next sought to identify C-terminal binding partners that might mediate these effects. Interrogation of our previously reported proteomic dataset generated in HEK293 cells expressing GFP-CdGAP identified the LIM domain containing protein LIMD1 as a prominent candidate interactor [7] (Supplementary Fig. 6A). We then validated the interaction between endogenous CdGAP and LIMD1 in MDA-MB-231 cells (Fig. 4A). To determine which region of CdGAP interacted with LIMD1, we co-immunoprecipitated GFP-tagged CdGAP deletion constructs and LIMD1 from HEK293 cell lysates (Fig. 4B, C). Both CdGAP full length and the C-terminus only (1160-1425) showed interaction with LIMD1, unlike the CdGAP mutant lacking the C-terminal region (1-820) (Fig. 4B, C). Given that the C-terminus of CdGAP has been

reported to interact with the protein Ajuba, a member of the LIM domain containing protein family through the residues R1172 and R1412 [44], we assessed the interaction of LIMD1 with the CdGAP point mutants in the C-terminal tail. We found that only R1172 is required to mediate the interaction between the C-terminus of CdGAP and LIMD1 (Fig. 4D). To map the reciprocal binding region in LIMD1, we expressed Xpress-tagged LIMD1 deletion constructs together with GFP-CdGAP in HEK293 cells. CdGAP interacted with full-length LIMD1 and the LIM domains, but not with the pre-LIM region of LIMD1 (Fig. 4B, E), demonstrating that the CdGAP C-terminus associates with the LIM domains of LIMD1.

CdGAP and LIMD1 co-regulate TNBC cell migration, morphology and focal adhesion dynamics

Because we identified LIMD1 as a CdGAP C-terminal interactor, we next asked whether LIMD1 contributes to CdGAP-dependent regulation of TNBC cell migration and focal adhesion dynamics. LIMD1 has been reported to modulate cell migration in a context-dependent manner [45-47], and both LIMD1 and CdGAP localize to focal adhesions, where they regulate adhesion dynamics in response to biophysical forces [48, 49]. We therefore generated monoclonal MDA-MB-231 cell lines with single depletion of LIMD1, as well as double LIMD1/CdGAP knock-out (KO) cells, to examine their functional interplay (Supplementary Fig. 6B). Similar to CdGAP KO cells, depletion of LIMD1 resulted in reduced cell migration. Double CdGAP/LIMD1 KO cell lines also exhibited reduced wound closure at similar rates as LIMD1 KO cell lines with no evidence of a synergistic effect (Fig. 4F and Supplementary Fig. 6C, D). LIMD1 KO cells also phenocopied CdGAP KO cells morphologically, displaying increased cell area and reduced aspect ratio compared to control cells (Fig. 4G-I and Supplementary Fig. 7A). Despite that CdGAP/LIMD1 double KO cells presented no significant changes in average cell area, they

exhibited a rounder and less elongated morphology, resulting in a reduced aspect ratio relative to control cells (Fig. 4G-I and Supplementary Fig. 7A). To further explore the relationship between CdGAP and LIMD1 at focal adhesions, we re-expressed GFP-CdGAP in CdGAP KO1 cells. GFP-CdGAP expression reduced cell spreading and co-localized with vinculin and endogenous LIMD1 at focal adhesions (Supplementary Fig. 7B and C). Notably, LIMD1 redistributed from a more diffuse cytoplasmic pattern to focal adhesions in GFP-CdGAP-expressing cells (Supplementary Fig. 7C), consistent with CdGAP promoting LIMD1 accumulation at these structures. We next investigated the dynamics of adhesion complexes by vinculin immunostaining in MDA-MB-231 CdGAP and LIMD1 KO cell lines. Both CdGAP and LIMD1 KO cells lacked the prominent protrusive edges and exhibited an increased number of adhesion complexes per cell (Fig. 4I, J and Supplementary Fig. 7A). In contrast, double CdGAP/LIMD1 KO cells showed a marked reduction in adhesion complexes together with an absence of protrusive areas (Fig. 4I, J and Supplementary Fig. 7A). Taken together, these findings indicate that CdGAP and LIMD1 functionally cooperate to regulate TNBC cell morphology, migration, and focal adhesion complex dynamics.

Loss of CdGAP and its C-terminus converge on a shared transcriptional program enriched for WNT signaling

Given that loss of CdGAP and truncation of its C-terminus produced similar defects in proliferation, morphology, migration, invasion, and metastatic potential, we asked whether these phenotypes were associated with disruption of a common transcriptional program in TNBC cells. We therefore performed transcriptomic analyses in MDA-MB-231 CdGAP KO1 and KI1 cell lines. Differential expression analysis identified 958 upregulated and 455 downregulated transcripts in CdGAP KO1 cells (Fig. 5A and Supplementary Table 5), and 879 upregulated and 477 dowregulated transcripts in CdGAP KI1 cells relative to control cells (Fig. 5B and Supplementary Table 5). Notably, 697 differentially expressed genes were shared between CdGAP KO1 and KI1 cells (Fig. 5C), indicating that the C-terminal region accounts for a substantial portion of the CdGAP-dependent transcriptional program in MDA-MB-231 cells.

At the pathway level, both datasets showed broad changes in programs linked to proliferation, metabolism, and cell organization, consistent with the phenotypic defects observed in CdGAP-deficient and C-terminally truncated cells (Supplementary Fig. 8A and B). In CdGAP KI1 cells, gene sets enrichment analysis revealed depleted signatures related to cell cycle progression, metabolism, intracellular signaling, and polarity/migration, together with enrichment of interferon response pathways (Supplementary Fig. 8A). Gene ontology analysis further highlighted altered extracellular matrix (ECM) organization, and we validated the reduced expression of the ECM-associated membrane-type matrix metalloproteinases 14 and 16 (*MMP14 and MMP16*) in CdGAP KI cells (Supplementary Fig. 8C and D). Since ECM remodelers are essential for tumor invasion and metastasis [50, 51], these results suggest that the CdGAP C-

terminus contributes to ECM-remodeling programs that control the proliferative and invasive behavior of TNBC cells.

Among the shared transcriptional alterations, WNT signaling emerged as a common and biologically relevant node. Over-representation analysis of differential genes shared between CdGAP KO1 and KI1 cells identified enrichment of the WNT signaling pathway (Fig. 5D and Supplementary Fig. 8E), and several WNT regulators were commonly altered, including the increased expression of *KREMEN1*, a membrane-associated inhibitor of the pathway (Fig. 5E). Together, these results indicate that the CdGAP C-terminus is required for much of the CdGAP-dependent transcriptional output in TNBC cells and identify dysregulation of a shared WNT signaling program as a candidate mechanism linking CdGAP to TNBC progression.

The CdGAP C-terminus promotes canonical WNT signaling in TNBC

Given the well-established role of canonical WNT signaling pathway in breast cancer cell proliferation, metastasis, stemness and drug resistance [52], we next investigated whether CdGAP regulates this pathway in TNBC. Because DKK1 and KREMEN1 cooperate to inhibit WNT signaling by inducing the endocytosis of the co-receptor LRP6 [53] (Fig. 6A), we first examined whether CdGAP and its C-terminal region influence LRP6 cell-surface levels. CdGAP KO and KI cells showed significantly lower basal levels of LRP6 at the cell surface than control cells (Fig. 6B, C). Upon stimulation with L-WRN conditioned medium (CM) [21], control cells showed the expected increase in cell-surface LRP6, whereas CdGAP KO and KI cells failed to respond (Fig. 6B, C). Consistent with these findings, both CdGAP KO and KI cells showed reduced accumulation of active β-catenin (non-phosphorylated at Ser33/37/Thr41)[54] following L-WRN CM stimulation compared to control cells (Fig. 6D, E). Likewise, canonical WNT transcriptional output, measured by TCF/LEF reporter activity and the expression of the WNT target gene *Axin-*

546 *2* [55], was significantly reduced in CdGAP KO and KI cells under stimulated conditions (Fig. 6F,
547 G). Together, these results indicate that CdGAP, through its C-terminal region, promotes canonical
548 WNT signaling in TNBC, at least in part by suppressing expression of the WNT inhibitor
549 KREMEN1 and thereby sustaining LRP6 cell-surface availability.

550 We next asked whether the interaction between LIMD1 and the CdGAP C-terminus
551 modulates this WNT-promoting function. Overexpression of the wild-type (WT) CdGAP in MDA-
552 MB-231 or HEK293 cells did not significantly alter WNT transcriptional activity under L-WRN
553 CM-stimulated conditions compared with empty vector (EV) controls (Fig. 6H and Supplementary
554 Fig. 9A-C). In contrast, expression of the LIMD1-binding-deficient mutant CdGAP-R1172A (Fig.
555 4D) significantly increased WNT transcriptional activity in both cell types following L-WRN CM
556 stimulation (Fig. 6H and Supplementary Fig. 9A-C). Taken together, these findings demonstrate
557 that LIMD1 binding to the CdGAP C-terminus restrains the ability of CdGAP to activate canonical
558 WNT signaling.

The CdGAP-dependent WNT transcriptional signature is associated with poor clinical outcomes in TNBC

To assess the clinical relevance of CdGAP-mediated regulation of the WNT signaling in TNBC, we derived a CdGAP-dependent WNT pathway signature based on the 18 genes identified in the GO analysis (Supplementary Fig. 8E and F). We then applied this signature to publicly available TNBC patient cohorts. Kaplan-Meier analysis of the MBC cohort revealed that high CdGAP-dependent WNT signature score was significantly associated with shorter time to metastasis (n=51, $p=3.2X10^{-4}$; Fig. 7A) [20]. This association was independently validated in the Jézéquel cohort (GSE58812; n=107) [18] in which a high signature score also predicted shorter time to metastasis (p=0.001; Fig. 7B) and reduced overall survival (p=0.0073; Fig. 7C). Similarly, in the Brueffer cohort (GSE96058) [19], a high CdGAP-dependent WNT signature score was associated with poorer overall survival (n=314, p=0.0016; Fig. 7D). Together, these findings support the clinical relevance of the CdGAP-dependent WNT transcriptional program in TNBC and suggest that activation of this pathway is associated with aggressive disease and adverse patient outcomes.

Discussion

Given the increased risk of death from recurrent disease and the lack of targeted therapies in TNBC [2], the identification of emerging oncogenic drivers is critical for advancing precision medicine. CdGAP has been previously established as a promoter of HER2-driven tumorigenesis and metastasis [7]. In addition, the congenital abnormalities in AOS patients bearing *CdGAP/ARHGAP31* truncating mutations may result from disruptions in cell proliferation and migration due to the loss of the C-terminus, a key region for post-translational modifications and protein interactions that regulate CdGAP activity [9, 44, 56]. This suggests that the C-terminus may contribute to the oncogenic properties of CdGAP and could be targeted in breast cancer therapeutics. In the present study, we established a CdGAP knock-in HER2+ mouse model, corresponding to the human *CDGAP-Q683X* AOS variant, to examine the contribution of the C-terminus to HER2+ breast tumorigenesis and metastasis. Although the deletion of the C-terminus induced a minor delay of tumor onset for $Neu^{+}CdGAP^{ki/ki}$ mice, it did not affect the formation and differentiation state of the primary tumors. This is in contrast with the complete deletion of CdGAP in the *MMTV-NIC* mouse model, which resulted in significant decreased tumor multiplicity [7]. Strikingly, the deletion of the C-terminus inhibited HER2-driven intravasation and lung metastasis, similar to the complete loss of CdGAP in HER2-driven metastasis to the lungs [7]. Therefore, this study provide evidence that the C-terminus is specifically required for the invasive ability of CdGAP to promote lung metastasis in HER2+-driven metastasis *in vivo*.

Given the clinical relevance of CdGAP in TNBC and the high expression of CdGAP mRNA levels in TNBC patient cell lines, we next developed a cellular model to characterize the response of TNBC cells to the absence of CdGAP or to the loss of the C-terminal region in critical processes associated with tumorigenesis and metastasis. Our findings demonstrate that 1) loss of the CdGAP

C-terminus produces a loss-of-function phenotype in TNBC cells, altering cell morphology, reducing proliferation, enhancing cell-cell adhesion, and impairing migration, invasion, and lung metastatic colonization; 2) CdGAP and its newly identified C-terminal interactor, LIMD1, co-regulate cell morphology, migration, and focal adhesion dynamics; 3) through its C-terminus, CdGAP regulates a WNT-associated transcriptional program in TNBC and acts as a positive regulator of the canonical WNT/β-catenin signaling; 4) LIMD1 binding to the CdGAP C-terminus restrains the ability of CdGAP to activate WNT signaling pathway; and 5) a CdGAP-dependent WNT transcriptional signature is associated with metastatic progression and poor overall survival in patients with TNBC. Therefore, this study reveals a pro-invasive domain (PID) at the C-terminus of CdGAP responsible for controlling TNBC cellular dynamics, metastasis, and activation of the WNT signaling pathway (Fig. 8).

Cancer cells can undergo EMT and acquire invasive and proliferative capabilities. Our findings demonstrate that CdGAP-depleted cells display epithelial-like characteristics, such as increased cell area, decreased elongation, and enhanced cell-cell contacts, consistent with global gene expression changes. This is in good agreement with previous studies showing that CdGAP also influenced EMT marker expression and cell adhesion, with its PRD interacting with ZEB2 to repress E-cadherin expression [6, 8]. In CdGAP KI MDA-MB-231 cells, expressing CdGAP lacking a complete PRD, we observed a decreased EMT-related gene signature expression and stronger cell-cell interactions in 3D culture. In the present study, we show that the loss of CdGAP reduced cell cycle-related and DNA repair pathways hallmarks, an effect that was consistently observed in prostate cancer PC-3 cells and HER2+ breast cancer cells, suggesting a conserved role for CdGAP in promoting cell cycle progression and maintaining genomic stability across different cancer types [6, 8]. Moreover, these pathways were altered to a similar extent in MDA-MB-231

cells expressing CdGAP lacking the C-terminal region. In patient-derived fibroblasts with the truncating mutation p.Gln683X, cell proliferation was also compromised [9]. These findings are consistent with our results, which demonstrate that CdGAP through its C-terminal region promotes cell proliferation, potentially through the regulation of G1 cell cycle progression. Of interest, one of the top hallmark in CdGAP KO MDA-MB-231 cells, and not present in the CdGAP KI MDA-MB-231 cells, was gene sets associated with TNFα signaling and NF-κB pathway, which strongly aligns with a recent study showing CdGAP as a novel transcriptional target and regulator of TNFα-induced nuclear localization of the NF-κB transcriptional protein RELA in pancreatic ductal adenocarcinoma (PDAC) cell lines [57]. These findings highlight potential context-dependent roles for CdGAP beyond its C-terminal functions, warranting further investigations in diverse cancer models.

In TNBC cells, the loss of CdGAP or its C-terminus led to increased cell-cell adhesion and impaired cell migration and invasion, which could be restored by re-expressing CdGAP. In good agreement with these results, CdGAP downregulation in prostate and HER2+ breast cancer cells significantly reduced cell migration and invasion regulated by TGF-β in HER2+ cells [6-8, 10]. CdGAP was also shown to play a key role in the control of directional membrane protrusions in migrating osteosarcoma U2OS cells [49, 58]. Moreover, the *in vivo* findings, together with the *in vitro* data, show that loss of CdGAP or its C-terminal region reduces lung metastatic burden in both the HER2+ mouse model and in tail vein injection using TNBC cells. In previous studies, we showed that CdGAP was required at multiple steps of HER2+-driven metastasis to the lungs and was required to promote distant metastasis to the intestine and bones in an orthotopic prostate cancer mouse model [6-8]. Altogether, these findings point to a crucial role of CdGAP as a pro-metastatic biomarker in prostate cancer and in the most aggressive breast cancer HER2+ and

643 TNBC subtypes. Likewise, our findings highlight the potential of targeting the C-terminal domain
644 of CdGAP as therapeutic strategy to inhibit breast cancer metastasis.

645 Interestingly, we identified LIMD1 as a novel protein binding to the C-terminus of CdGAP.
646 Previous studies have demonstrated the interaction between CdGAP and another LIM-containing
647 protein AJUBA [44]. Here we validated that the residue R1172 located at the C-terminus of
648 CdGAP mediates the interaction with LIM domains. Additionally, loss of LIMD1 in MDA-MB-
649 231 cells resulted in a similar phenotype to the depletion of CdGAP, showing decreased cell
650 migration while exhibiting epithelial-like characteristics. The interaction between the LIM
651 domains of AJUBA and the CdGAP C-terminus inhibited its GAP activity, stabilizing cell-cell
652 junctions. Moreover, expression of the AOS mutant lacking the C-terminal region failed to
653 maintain cell junction integrity in keratinocytes [44]. In contrast, in TNBC cells, we observed that
654 both CdGAP KO and KI TNBC cell lines presented increased cell-cell interactions. This suggests
655 that in cancer cells, CdGAP might have different roles in regulating cell-cell junction dynamics,
656 and by interacting with LIMD1, they both contribute to cell migration. CdGAP and LIMD1 have
657 emerged as significant players in mechano-transduction, modulating focal adhesion formation and
658 cell migration [7, 48, 49]. Here we show that CdGAP and LIMD1 co-localize at sites of focal
659 adhesion complexes in MDA-MB-231 cells. Furthermore, depleted CdGAP and LIMD1 cells
660 presented cell elongation defects as well as decreased cell migration and focal adhesion formation,
661 demonstrating that the cooperative interaction between CdGAP and LIMD1 is crucial for
662 maintaining adequate focal adhesion dynamics for effective cell migration in TNBC cells.

663 ECM degradation is critical to facilitate cell migration and invasion during metastasis. We
664 observed a significant decrease in these cellular processes, along with changes in ECM-related
665 pathways and metastatic patterns in MDA-MB-231 cells expressing CdGAP lacking the C-

terminus. Additionally, we validated the downregulation of *MMP-14* and *MMP-16*, which activate pro-MMP-2 and degrade ECM components including fibronectin, laminin, and collagen [59]. MMP-14 is associated with poor prognosis, while MMP-16 is linked with better survival, but may contribute to drug resistance [60-64]. These findings suggests that CdGAP C-terminus plays a role in regulating breast cancer cell migration, invasion and metastasis through mechanisms controlling ECM degradation.

In TNBC, the hallmark enhancement of the WNT/β-catenin pathway is associated with poor clinical outcome [65], by promoting tumorigenesis and metastasis [66, 67]. In this study, global gene expression analysis uncovered a common WNT signaling pathway signature in MDA-MB-231 cells depleted of CdGAP and in CdGAP KI expressing cells. The loss of CdGAP, or of its C-terminal region resulted in increased expression of the WNT negative regulator KREMEN1, accompanied by inhibition of LRP6 at the cell surface. Moreover, our results demonstrate that the C-terminal region plays a critical role in the activation of β-catenin and WNT transcriptional activity in response to WNT external stimuli. Interestingly, the mutant CdGAP-R1172A lacking the ability to interact with LIMD1 behaved as a dominant positive mutant, leading to increased activation of the WNT transcriptional activity. Given that LIMD1 and CdGAP interact at focal adhesions (Fig. 8), it is likely that the ability of LIMD1 to undergo phase-separation driven by mechanical forces [48] recruits CdGAP within adhesion condensate, thereby contributing to focal adhesion dynamics while limiting the ability of CdGAP to positively regulate the WNT signaling pathway. Notably, LIMD1 has also been shown as a negative regulator of canonical Wnt pathway in differentiating osteoblasts [68]. Importantly, analysis of three independent gene expression datasets from patients with TNBC revealed that the CdGAP-regulated WNT signaling signature is associated with shorter time to metastasis and poorer overall survival, highlighting the potential

role of CdGAP-mediated WNT signaling in TNBC progression. In previous studies, we have reported a TGFβ-EMT gene signature regulated by CdGAP in HER2+ breast tumors and breast cancer cell lines [6, 7], suggesting that CdGAP may regulate two distinct sets of pathways, TGFβ and WNT, in HER2+ and TNBC, respectively. Emerging evidence suggests that alterations in the activation of the WNT pathway rather than mutations in the β-catenin gene contribute to the metastatic potential of TNBC [67]. Current efforts to target the WNT/β-catenin pathway in breast cancer have resulted in the study of monoclonal antibodies, natural compounds and small molecule inhibitors. However, these studies are still in the early phase of clinical trials [69-71]. There remains a need to develop more effective strategies to inhibit the WNT pathway, which could ultimately improve treatment outcomes for patients with TNBC.

The complex network of signaling pathways and cellular processes, including WNT/β-catenin, TGFβ-driven EMT, ECM remodeling, focal adhesion dynamics, and Rho GTPase signaling, collectively promotes an invasive phenotype in HER2+ and TNBC tumors with mesenchymal features. Altogether, our findings establish the CdGAP C-terminal region as a pro-invasive driver of breast cancer metastasis and highlight its potential as a therapeutic target. These results open new avenues of combination strategies involving WNT inhibitors, with the goal of enhancing the efficacy of existing therapies and improving the management of TNBC metastasis.

Acknowledgements

We thank Ms. Marie-Hélène Lacombe, Hélène Pagé-Veillette and Ekaterina Lourtchenko at the immunophenotyping platform of the RI-MUHC. We thank Dr. Min Fu and Ms. Chibo Feng at the molecular imaging platform of the RI-MUHC. We also thank the Molecular Biology and Functional Genomics core facility for generating the libraries for RNA sequencing and Ms. Fazila Chouiali at the histopathology platform of the RI-MUHC. Our acknowledgments to Dr. Tyson V. Sharp for giving us the Xpress-tagged LIMD1 constructs. M.-L.M. was supported by a doctoral studentship offered by National Council of Science and Technology (Consejo Nacional de Ciencia y Tecnologia CONACyT), the Merit Scholarship Program for Foreign Students (PBEEE) offered by the Quebec Research Fund-Nature and Technologies (FRQNT), the Resident Type Tuition Program of the Government of the Province of Quebec offered by the Ministry of Education and Higher Education of Quebec (MEES) and the Mexican Agency of International Cooperation for Development (AMEXCID), and the Bourse Michel-Lessard. J.C. was supported by the Peter Quinlan fellowship in oncology. N. A. and E. J. M. held a MITACS Globalink internship award. D.P.L. is a William Dawson Scholar of McGill University, a Lewis Katz – Young Investigator of the Prostate Cancer Foundation, and a Research Scholar – Senior from the Fonds de recherche du Québec-Santé. This research was supported by CIHR project grants to D.P.L (PJT-180368; PJT-203949) and N.L.-V (PJT-153151; PJT-180367).

Authors' Contributions

Conceptualization, MLM and NLV; data acquisition, MLM, NB, YH, JC, JAR, EJM, NA; methodology, MLM, NB, YH; validation, MLM, NB, YH, DPL, NLV; formal analysis, MLM, NB, YH, DPL, NLV; resources, AG; writing-original draft, MLM and NLV; writing-review and editing, MLM, NB, YH, AG, DPL, NLV; funding acquisition, DPL and NLV.

References

1 Giaquinto AN, Sung H, Miller KD, Kramer JL, Newman LA, Minihan A *et al*. Breast Cancer Statistics, 2022. *CA Cancer J Clin* 2022; 72: 524-541.

2 Yin L, Duan JJ, Bian XW, Yu SC. Triple-negative breast cancer molecular subtyping and treatment progress. *Breast Cancer Res* 2020; 22: 61.

3 Tcherkezian J, Lamarche-Vane N. Current knowledge of the large RhoGAP family of proteins. *Biol Cell* 2007; 99: 67-86.

4 Kreider-Letterman G, Carr NM, Garcia-Mata R. Fixing the GAP: The role of RhoGAPs in cancer. *Eur J Cell Biol* 2022; 101: 151209.

5 Lamarche-Vane N, Hall A. CdGAP, a novel proline-rich GTPase-activating protein for Cdc42 and Rac. *J Biol Chem* 1998; 273: 29172-29177.

6 He Y, Northey JJ, Pelletier A, Kos Z, Meunier L, Haibe-Kains B *et al*. The Cdc42/Rac1 regulator CdGAP is a novel E-cadherin transcriptional co-repressor with Zeb2 in breast cancer. *Oncogene* 2017; 36: 3490-3503.

7 He Y, Goyette MA, Chapelle J, Boufaied N, Al Rahbani J, Schonewolff M *et al*. CdGAP is a talin-binding protein and a target of TGF-beta signaling that promotes HER2-positive breast cancer growth and metastasis. *Cell Rep* 2023; 42: 112936.

8 Mehra C, Chung JH, He Y, Lara-Marquez M, Goyette MA, Boufaied N *et al*. CdGAP promotes prostate cancer metastasis by regulating epithelial-to-mesenchymal transition, cell cycle progression, and apoptosis. *Commun Biol* 2021; 4: 1042.

9 Southgate L, Machado RD, Snape KM, Primeau M, Dafou D, Ruddy DM *et al*. Gain-of-function mutations of ARHGAP31, a Cdc42/Rac1 GTPase regulator, cause syndromic cutis aplasia and limb anomalies. *Am J Hum Genet* 2011; 88: 574-585.

10 He Y, Northey JJ, Primeau M, Machado RD, Trembath R, Siegel PM *et al*. CdGAP is required for transforming growth factor beta- and Neu/ErbB-2-induced breast cancer cell motility and invasion. *Oncogene* 2011; 30: 1032-1045.

11 Ursini-Siegel J, Hardy WR, Zuo D, Lam SH, Sanguin-Gendreau V, Cardiff RD *et al*. ShcA signalling is essential for tumour progression in mouse models of human breast cancer. *Embo j* 2008; 27: 910-920.

12 Laurin M, Huber J, Pelletier A, Houalla T, Park M, Fukui Y *et al*. Rac-specific guanine nucleotide exchange factor DOCK1 is a critical regulator of HER2-mediated breast cancer metastasis. *Proc Natl Acad Sci U S A* 2013; 110: 7434-7439.

13 Pereira B, Chin SF, Rueda OM, Vollan HK, Provenzano E, Bardwell HA *et al*. The somatic mutation profiles of 2,433 breast cancers refines their genomic and transcriptomic landscapes. *Nat Commun* 2016; 7: 11479.

14 Curtis C, Shah SP, Chin SF, Turashvili G, Rueda OM, Dunning MJ *et al*. The genomic and transcriptomic architecture of 2,000 breast tumours reveals novel subgroups. *Nature* 2012; 486: 346-352.

15 Cerami E, Gao J, Dogrusoz U, Gross BE, Sumer SO, Aksoy BA *et al*. The cBio cancer genomics portal: an open platform for exploring multidimensional cancer genomics data. *Cancer Discov* 2012; 2: 401-404.

16 Gao J, Aksoy BA, Dogrusoz U, Dresdner G, Gross B, Sumer SO *et al*. Integrative analysis of complex cancer genomics and clinical profiles using the cBioPortal. *Sci Signal* 2013; 6: pl1.

17 de Bruijn I, Kundra R, Mastrogiacomo B, Tran TN, Sikina L, Mazor T *et al*. Analysis and Visualization of Longitudinal Genomic and Clinical Data from the AACR Project GENIE Biopharma Collaborative in cBioPortal. *Cancer Res* 2023; 83: 3861-3867.

18 Jezequel P, Loussouarn D, Guerin-Charbonnel C, Campion L, Vanier A, Gouraud W *et al*. Gene-expression molecular subtyping of triple-negative breast cancer tumours: importance of immune response. *Breast Cancer Res* 2015; 17: 43.

19 Brueffer C, Vallon-Christersson J, Grabau D, Ehinger A, Hakkinen J, Hegardt C *et al*. Clinical Value of RNA Sequencing-Based Classifiers for Prediction of the Five Conventional Breast Cancer Biomarkers: A Report From the Population-Based Multicenter Sweden Cancerome Analysis Network-Breast Initiative. *JCO Precis Oncol* 2018; 2.

20 Wagle N, Painter C, Anastasio E, Dunphy M, McGillicuddy M, Kim D *et al*. The Metastatic Breast Cancer (MBC) project: Accelerating translational research through direct patient engagement. *Journal of Clinical Oncology* 2017; 35.

21 VanDussen KL, Sonnek NM, Stappenbeck TS. L-WRN conditioned medium for gastrointestinal epithelial stem cell culture shows replicable batch-to-batch activity levels across multiple research teams. *Stem Cell Res* 2019; 37: 101430.

22 LaLonde DP, Grubinger M, Lamarche-Vane N, Turner CE. CdGAP associates with actopaxin to regulate integrin-dependent changes in cell morphology and motility. *Curr Biol* 2006; 16: 1375-1385.

23 Foxler DE, Bridge KS, James V, Webb TM, Mee M, Wong SC *et al*. The LIMD1 protein bridges an association between the prolyl hydroxylases and VHL to repress HIF-1 activity. *Nat Cell Biol* 2012; 14: 201-208.

24 Veeman MT, Slusarski DC, Kaykas A, Louie SH, Moon RT. Zebrafish prickle, a modulator of noncanonical Wnt/Fz signaling, regulates gastrulation movements. *Curr Biol* 2003; 13: 680-685.

25 Ran FA, Hsu PD, Wright J, Agarwala V, Scott DA, Zhang F. Genome engineering using the CRISPR-Cas9 system. *Nat Protoc* 2013; 8: 2281-2308.

26 Lara-Marquez M, Báez-Magaña M, Raymundo-Ramos C, Spagnuolo PA, Macías-Rodríguez L, Salgado-Gargiglia R *et al*. Lipid-rich extract from Mexican avocado (Persea americana var. drymifolia) induces apoptosis and modulates the inflammatory response in Caco-2 human colon cancer cells. *Journal of Functional Foods* 2020; 64: 103658.

27 Lee YJ, Lin WL, Chen NF, Chuang SK, Tseng TH. Demethylwedelolactone derivatives inhibit invasive growth in vitro and lung metastasis of MDA-MB-231 breast cancer cells in nude mice. *Eur J Med Chem* 2012; 56: 361-367.

28 Bourgey M, Dali R, Eveleigh R, Chen KC, Letourneau L, Fillon J *et al*. GenPipes: an open-source framework for distributed and scalable genomic analyses. *Gigascience* 2019; 8.

29 Bolger AM, Lohse M, Usadel B. Trimmomatic: a flexible trimmer for Illumina sequence data. *Bioinformatics* 2014; 30: 2114-2120.

30 Dobin A, Davis CA, Schlesinger F, Drenkow J, Zaleski C, Jha S *et al*. STAR: ultrafast universal RNA-seq aligner. *Bioinformatics* 2013; 29: 15-21.

31 Van der Auwera GA, O'Connor BD. *Genomics in the Cloud*. O'Reilly Media, Inc., 2020.

32 Anders S, Pyl PT, Huber W. HTSeq--a Python framework to work with high-throughput sequencing data. *Bioinformatics* 2015; 31: 166-169.

33 Love MI, Huber W, Anders S. Moderated estimation of fold change and dispersion for RNA-seq data with DESeq2. *Genome Biol* 2014; 15: 550.

34 Wu T, Hu E, Xu S, Chen M, Guo P, Dai Z *et al*. clusterProfiler 4.0: A universal enrichment tool for interpreting omics data. *Innovation (Camb)* 2021; 2: 100141.

35 Yu G, Wang LG, Han Y, He QY. clusterProfiler: an R package for comparing biological themes among gene clusters. *OMICS* 2012; 16: 284-287.

36 Liberzon A, Birger C, Thorvaldsdottir H, Ghandi M, Mesirov JP, Tamayo P. The Molecular Signatures Database (MSigDB) hallmark gene set collection. *Cell Syst* 2015; 1: 417-425.

37 Agajanian MJ, Walker MP, Axtman AD, Ruela-de-Sousa RR, Serafin DS, Rabinowitz AD *et al*. WNT Activates the AAK1 Kinase to Promote Clathrin-Mediated Endocytosis of LRP6 and Establish a Negative Feedback Loop. *Cell Rep* 2019; 26: 79-93 e78.

38 Bhuva DD, Cursons J, Davis MJ. Stable gene expression for normalisation and single-sample scoring. *Nucleic Acids Res* 2020; 48: e113.

39 Govindarajulu U, Tarpey T. Optimal partitioning for the proportional hazards model. *J Appl Stat* 2022; 49: 968-987.

40 Therneau TM. A Package for Survival Analysis in R. *R package version 38-3* 2020; https://CRAN.R-project.org/package=survival.

41 Kassambara A, Kosinski M, Biecek P, Scheipl F. Drawing Survival Curves using 'ggplot2'. *R Package Version 046* 2016; http://CRAN.r-project.org/web/packages/survminer

42 Hassed S, Li S, Mulvihill J, Aston C, Palmer S. Adams-Oliver syndrome review of the literature: Refining the diagnostic phenotype. *Am J Med Genet A* 2017; 173: 790-800.

43 Yamazaki D, Kurisu S, Takenawa T. Regulation of cancer cell motility through actin reorganization. *Cancer Sci* 2005; 96: 379-386.

44 McCormack JJ, Bruche S, Ouadda ABD, Ishii H, Lu H, Garcia-Cattaneo A *et al*. The scaffold protein Ajuba suppresses CdGAP activity in epithelia to maintain stable cell-cell contacts. *Sci Rep* 2017; 7: 9249.

45 Sharp TV, Al-Attar A, Foxler DE, Ding L, de AVTQ, Zhang Y *et al*. The chromosome 3p21.3-encoded gene, LIMD1, is a critical tumor suppressor involved in human lung cancer development. *Proc Natl Acad Sci U S A* 2008; 105: 19932-19937.

46 Tang J, Zhu L, Huang Y, Shi B, Zhang S, Gu L *et al*. Silencing of LIMD1 promotes proliferation and reverses cell adhesion-mediated drug resistance in non-Hodgkin's lymphoma. *Oncol Lett* 2019; 17: 2993-3000.

47 Chakraborty C, Mitra S, Roychowdhury A, Samadder S, Dutta S, Roy A *et al*. Deregulation of LIMD1-VHL-HIF-1alpha-VEGF pathway is associated with different stages of cervical cancer. *Biochem J* 2018; 475: 1793-1806.

48 Wang Y, Zhang C, Yang W, Shao S, Xu X, Sun Y *et al*. LIMD1 phase separation contributes to cellular mechanics and durotaxis by regulating focal adhesion dynamics in response to force. *Dev Cell* 2021; 56: 1313-1325 e1317.

49 Wormer DB, Davis KA, Henderson JH, Turner CE. The focal adhesion-localized CdGAP regulates matrix rigidity sensing and durotaxis. *PLoS One* 2014; 9: e91815.

50 Jiang C, Wang J, Dong C, Wei W, Li J, Li X. Membranous type matrix metalloproteinase 16 induces human prostate cancer metastasis. *Oncol Lett* 2017; 14: 3096-3102.

51 Hillebrand LE, Wickberg SM, Gomez-Auli A, Follo M, Maurer J, Busch H *et al*. MMP14 empowers tumor-initiating breast cancer cells under hypoxic nutrient-depleted conditions. *FASEB J* 2019; 33: 4124-4140.

52 Hashemi M, Hasani S, Hajimazdarany S, Ghadyani F, Olyaee Y, Khodadadi M *et al*. Biological functions and molecular interactions of Wnt/beta-catenin in breast cancer: Revisiting signaling networks. *Int J Biol Macromol* 2023; 232: 123377.

53 Mao B, Wu W, Davidson G, Marhold J, Li M, Mechler BM *et al*. Kremen proteins are Dickkopf receptors that regulate Wnt/beta-catenin signalling. *Nature* 2002; 417: 664-667.

54 Liu J, Xiao Q, Xiao J, Niu C, Li Y, Zhang X *et al*. Wnt/beta-catenin signalling: function, biological mechanisms, and therapeutic opportunities. *Signal Transduct Target Ther* 2022; 7: 3.

55 Sun S, Gong YD, Kang JS, Dong MS, Choi Y. A small molecule compound 759 inhibits the wnt/beta-catenin signaling pathway via increasing the Axin protein stability. *Med Oncol* 2024; 41: 147.

56 Ben Djoudi Ouadda A, He Y, Calabrese V, Ishii H, Chidiac R, Gratton JP *et al*. CdGAP/ARHGAP31 is regulated by RSK phosphorylation and binding to 14-3-3beta adaptor protein. *Oncotarget* 2018; 9: 11646-11664.

57 Butera F, Sero JE, Dent LG, Bakal C. Actin networks modulate heterogeneous NF-kappaB dynamics in response to TNFalpha. *Elife* 2024; 13.

58 Wormer D, Deakin NO, Turner CE. CdGAP regulates cell migration and adhesion dynamics in two-and three-dimensional matrix environments. *Cytoskeleton (Hoboken)* 2012; 69: 644-658.

59 Itoh Y. Membrane-type matrix metalloproteinases: Their functions and regulations. *Matrix Biol* 2015; 44-46: 207-223.

60 McGowan PM, Duffy MJ. Matrix metalloproteinase expression and outcome in patients with breast cancer: analysis of a published database. *Ann Oncol* 2008; 19: 1566-1572.

61 Xia H, Yu W, Liu M, Li H, Pang W, Wang L *et al*. An integrated bioinformatics analysis of potential therapeutic targets among matrix metalloproteinases in breast cancer. *Oncol Lett* 2019; 18: 2985-2994.

62 Cheng T, Chen P, Chen J, Deng Y, Huang C. Landscape Analysis of Matrix Metalloproteinases Unveils Key Prognostic Markers for Patients With Breast Cancer. *Front Genet* 2021; 12: 809600.

63 Hermawan A, Putri H, Hanif N, Fatimah N, Prasetio HH. Identification of potential target genes of honokiol in overcoming breast cancer resistance to tamoxifen. *Front Oncol* 2022; 12: 1019025.

64 Oliveras-Ferraros C, Vazquez-Martin A, Cuyas E, Corominas-Faja B, Rodriguez-Gallego E, Fernandez-Arroyo S *et al*. Acquired resistance to metformin in breast cancer cells triggers transcriptome reprogramming toward a degradome-related metastatic stem-like profile. *Cell Cycle* 2014; 13: 1132-1144.

65 Khramtsov AI, Khramtsova GF, Tretiakova M, Huo D, Olopade OI, Goss KH. Wnt/beta-catenin pathway activation is enriched in basal-like breast cancers and predicts poor outcome. *Am J Pathol* 2010; 176: 2911-2920.

66 Dey N, Barwick BG, Moreno CS, Ordanic-Kodani M, Chen Z, Oprea-Ilies G *et al*. Wnt signaling in triple negative breast cancer is associated with metastasis. *BMC Cancer* 2013; 13: 537.

67 Geyer FC, Lacroix-Triki M, Savage K, Arnedos M, Lambros MB, MacKay A *et al*. beta-Catenin pathway activation in breast cancer is associated with triple-negative phenotype but not with CTNNB1 mutation. *Mod Pathol* 2011; 24: 209-231.

68 Luderer HF, Bai S, Longmore GD. The LIM protein LIMD1 influences osteoblast differentiation and function. *Exp Cell Res* 2008; 314: 2884-2894.

69 Rodon J, Argiles G, Connolly RM, Vaishampayan U, de Jonge M, Garralda E *et al*. Phase 1 study of single-agent WNT974, a first-in-class Porcupine inhibitor, in patients with advanced solid tumours. *Br J Cancer* 2021; 125: 28-37.

70 Diamond JR, Becerra C, Richards D, Mita A, Osborne C, O'Shaughnessy J *et al*. Phase Ib clinical trial of the anti-frizzled antibody vantictumab (OMP-18R5) plus paclitaxel in patients with locally advanced or metastatic HER2-negative breast cancer. *Breast Cancer Res Treat* 2020; 184: 53-62.

71 Maitland ML, Sachdev JC, Sharma MR, Moreno V, Boni V, Kummar S *et al*. First-in-Human Study of PF-06647020 (Cofetuzumab Pelidotin), an Antibody-Drug Conjugate Targeting Protein Tyrosine Kinase 7, in Advanced Solid Tumors. *Clin Cancer Res* 2021; 27: 4511-4520.

Figure Legends

Figure 1. The CdGAP C-terminus contributes to lung metastasis in a mouse HER2$^+$ breast cancer model

A, Schematic illustration of *MMTV-Neu* mice intercrossed with *CdGAP$^{ki/ki}$* mice and the cohort analysis experiments performed 5 weeks after tumor onset. **B**, PCR analysis on genomic DNA extracted from mammary tumors or tails. **C**, Representative immunoblots showing the expression of Neu, CdGAP wild-type (wt), and CdGAP knock-in (ki) lacking the C-terminus in tumors from *Neu$^+$CdGAP$^{wt/wt}$* and *Neu$^+$CdGAP$^{ki/ki}$* mice. α-Tubulin was used as a loading control. **D**, Tumor-free incidence was analyzed over time (n=25-29 mice, *p=0.014). $T_{1/2}$ represents the age (days) at which 50% of the mice had palpable mammary tumors. **E**, Quantification of Mammary Intraepithelial Neoplastic (MIN) lesions from *Neu$^+$CdGAP$^{wt/wt}$* and *Neu$^+$CdGAP$^{ki/ki}$* mice 5 weeks after tumor onset (n=8-11mice). ns, not significant. **F and G**, Quantification of tumor mass (**F**) and number of primary tumor (**G**) in individual mouse (n=25-29 mice). ns, not significant. **H**, Representative images of lung sections stained with H&E. scale bar, 100 μm. **I**, Lung metastasis frequency was analyzed amongst indicated groups (n=16-22 mice, ****p < 0.0001, Chi-square test). **J**, Quantification of total number of lung metastasis per mouse (n=16-22 mice, *p=0.03, **p=0.004). **K**, Schematic illustration of the intravasation assay and quantification of circulating tumor cell (CTC) number in individual mouse per blood volume (ml) per tumor weight (g) (n=5 mice, **p=0.0085).

Figure 2. CdGAP depletion and loss of the C-terminal region affects cell morphology and increases cell-cell adhesions in TNBC cells. A, Expression (log 2 (transcripts per million +1)) of *ARHGAP31* in human breast cancer cell lines from the Expression Public 23Q4 project via the DepMap portal. **B**, Schematic illustration of CdGAP wild type (WT) and CdGAP mutant

(p.Gln683X) identified in patients with the Adams-Oliver syndrome (AOS). PBR= Polybasic region, GAP= GTPase-activating protein, BR= Basic region, PRD= Proline rich domain. Representative immunoblots showing the expression of CdGAP WT and CdGAP KI lacking the C-terminus in monoclonal cell lines (CdGAP KO1, KO2, KI1, KI2) originated from control (Ctl) MDA-MD-231 and HS578T. **C,** Representative immunofluorescence images of control (Ctl), CdGAP KO and KI MDA-MB-231 cell lines cultured on fibronectin coated coverslips and analyzed by confocal microscopy. F-actin and nuclei staining was done with phalloidin-TRITC and DAPI, respectively. Scale bars, 100 μm (top images) and 50 μm (bottom images). **D and E**, Quantification of the cell area **(D)** and cell length **(E)** from (C)**. F,** Representative immunofluorescence images of control (Ctl), CdGAP KO and KI MDA-MB-231 spheroids stained with phalloidin-TRITC and DAPI. Scale bar represents 100 μm. **G and H**, Graphs representing spheroid area **(G)** in fold change and solidity (area/convex area) **(H)** are presented. Data are presented as mean ± SEM (***$p < 0.001$, ****$p < 0.0001$, ns, not significant).

Figure 3. The CdGAP C-terminus is required to promote TNBC cell migration, invasion, and metastasis. A and B, Cells were cultured on poly-D-lysine–coated plates, followed by the formation of a wound and analysis of wound closure over time. Quantification of relative wound confluence over 15 hours in the indicated MDA-MB-231 **(A)** and HS578T **(B)** cell lines. Multiple unpaired t test results for the individual time points are shown in Supplementary Figure S4B and D. **C-F,** Quantification of transwell migration and invasion assays of MDA-MB-231 **(C and D)** and HS578T **(E and F)** cell lines. **G,** Immunoblots showing the transfection of the CdGAP KO1 MDA-MB-231 cells with empty vector (EV) or myc-CdGAP. **H,** Representative images of transwell migration assays of cells transfected as in (G), Scale bar, 500 μm. **I,** Quantification of transwell migration assays of cells transfected in (G). **J,** Schematic illustration of the experimental

workflow to assess lung colonization *in vivo*. CdGAP KO and KI MDA-MB-231 cells were injected into the tail vein of immunocompromised mice. After 5 weeks, lungs were collected and analyzed by H&E staining to evaluate metastatic burden. **K,** Quantification of the number of lung metastasis per mice. Data are presented as mean ± SEM (*p < 0.05, ** p < 0.01, ***p < 0.001, **** p < 0.0001, ns, not significant).

Figure 4. CdGAP and its C-terminal interactor LIMD1 co-regulate cell morphology, migration and focal adhesion dynamics. A, CdGAP was immunoprecipitated (IP) from MDA-MB-231 protein lysates with anti-CdGAP antibodies or rabbit immunoglobulin G (IgG) as negative control. TCL: total cell lysates. **B,** Schematic illustration of CdGAP and LIMD1. PBR= polybasic region, GAP= GTPase-activating protein, BR= basic region, PRD= proline-rich domain. **C-E,** HEK293 cells were transfected with the indicated constructs, followed by GFP **(C and D)** or X-press **(E)** immunoprecipitation (IP) and immunoblotting. TCL, total cell lysate. **F,** Quantification of relative wound confluence over 15 hours in the indicated MDA-MB-231 cell lines. **G-J,** MDA-MB-231 cell lines cultured on fibronectin coated coverslips and analyzed by confocal microscopy. Quantification of the cell area **(G)** and aspect ratio **(H)** from representative images **(I)** for vinculin (green), F-actin (red), and nuclei staining (blue). Scale bar, 30 μm. **J,** Quantification of the number of adhesion complexes per cell. Data are presented as mean ± SEM (*p < 0.05, ***p < 0.001, **** p < 0.0001, ns, not significant).

Figure 5. CdGAP and its C-terminal region regulates a common WNT signaling pathway signature in MDA-MB-231 cells. A and B, Volcano plot depicting the differentially expressed genes between control (Ctl) and **(A)** CdGAP KO1 or **(B)** KI1 MDA-MB-231 cells with their respective heatmap portraying differentially expressed genes. Red dots represent genes with an absolute fold change (FC) >1 ($log_2FC=1$) and $p < 0.05$. **C,** Venn diagram illustrating the overlap

of differentially expressed genes between CdGAP KO1 and KI1 analyses. Analysis was performed using only gene ID symbols. **D,** Barplot showing over-representation analysis performed on shared differential genes in CdGAP KO1 and KI1. Only the significantly enriched WNT signaling gene set are shown. **E,** Heatmap portraying the leading-edge genes contributing to the enrichment of the WNT signaling pathway common to both CdGAP KO1 and KI1 cells.

Figure 6. CdGAP activates the WNT signaling pathway through its C-terminal domain in MDA-MB-231 cells. A, Schematic illustration of the inhibitory mechanism of the membrane proteins DKK1 and KREMEN1 of the canonical WNT pathway. **B,** Representative histograms of flow cytometry assays using anti-LRP6 or the isotype control (IgG) antibodies in CdGAP KO and KI MDA-MB-231 cells stimulated for 24 h with 5% conditioned medium (CM) L-WRN (+) or in cells left unstimulated (-). **C,** Quantification of LRP6 at the cell surface relative to IgG. **D,** Representative immunoblots showing the activation of β-catenin (non-phosphorylated at Ser33/37/Thr41) in the indicated cell lines stimulated with conditioned medium (CM) L-WRN (+) or left unstimulated (-). **E,** Quantification of active β-catenin relative to unstimulated control. **F,** WNT transcriptional luciferase assays. **G,** Quantification of Axin-2 mRNA levels. **H,** WNT transcriptional luciferase assays in MDA-MB-231 cells transfected with GFP-empty vector (EV), GFP-CdGAP wild type (WT) or GFP-CdGAP-R1172A, stimulated with 5% conditioned medium (CM) L-WRN (+) or left unstimulated (-). Data are presented as mean ± SEM (*$p < 0.05$, **$p < 0.01$, ***$p < 0.001$, ****$p < 0.0001$, ns, not significant). In **E-G,** only statistically significant comparisons are shown, and full statistical analysis are provided in Supplementary Table 6.

Figure 7. CdGAP-dependent WNT transcriptional signature predicts poor clinical outcomes in TNBC patients. A and B, Kaplan-Meier curve of the time to metastasis of TNBC patients for the MBC cohort RNAseq dataset (n=51, $p=3.2X10^{-4}$) **(A)** and the Jézéquel cohort (GSE58812) microarray dataset (n=107, p= 0.001) **(B)** based on the WNT signature from CdGAP KO1 MDA-MB-231 cells (Supplementary Fig. S8E and F). **C and D,** Kaplan-Meier curve of the overall survival probability of TNBC patients for the Jézéquel cohort (GSE58812) microarray dataset (n=107, p= 0.0073) **(C)** and the Brueffer cohort (GSE96058) RNAseq dataset (n=314, p=0.0016) **(D)** based on the WNT signature from CdGAP KO1 MDA-MB-231 cells (Supplementary Fig. 8E, F).

Figure 8. A pro-invasive domain (PID) at the C-terminus of CdGAP controls breast cancer progression and activates the canonical WNT/β-catenin signaling pathway in TNBC. In this study, we have identified a pro-invasive domain (PID) at the C-terminus of CdGAP interacting with LIMD1 to regulate focal adhesion formation, actin cytoskeletal dynamics, and cell migration. In addition, the C-terminal PID regulates a WNT signaling pathway gene signature and modulates TNBC cellular dynamics and metastasis. The interaction of LIMD1 and the C-terminal PID contributes to fine-tuning the regulation of the WNT signaling pathway in TNBC.

Figure 1

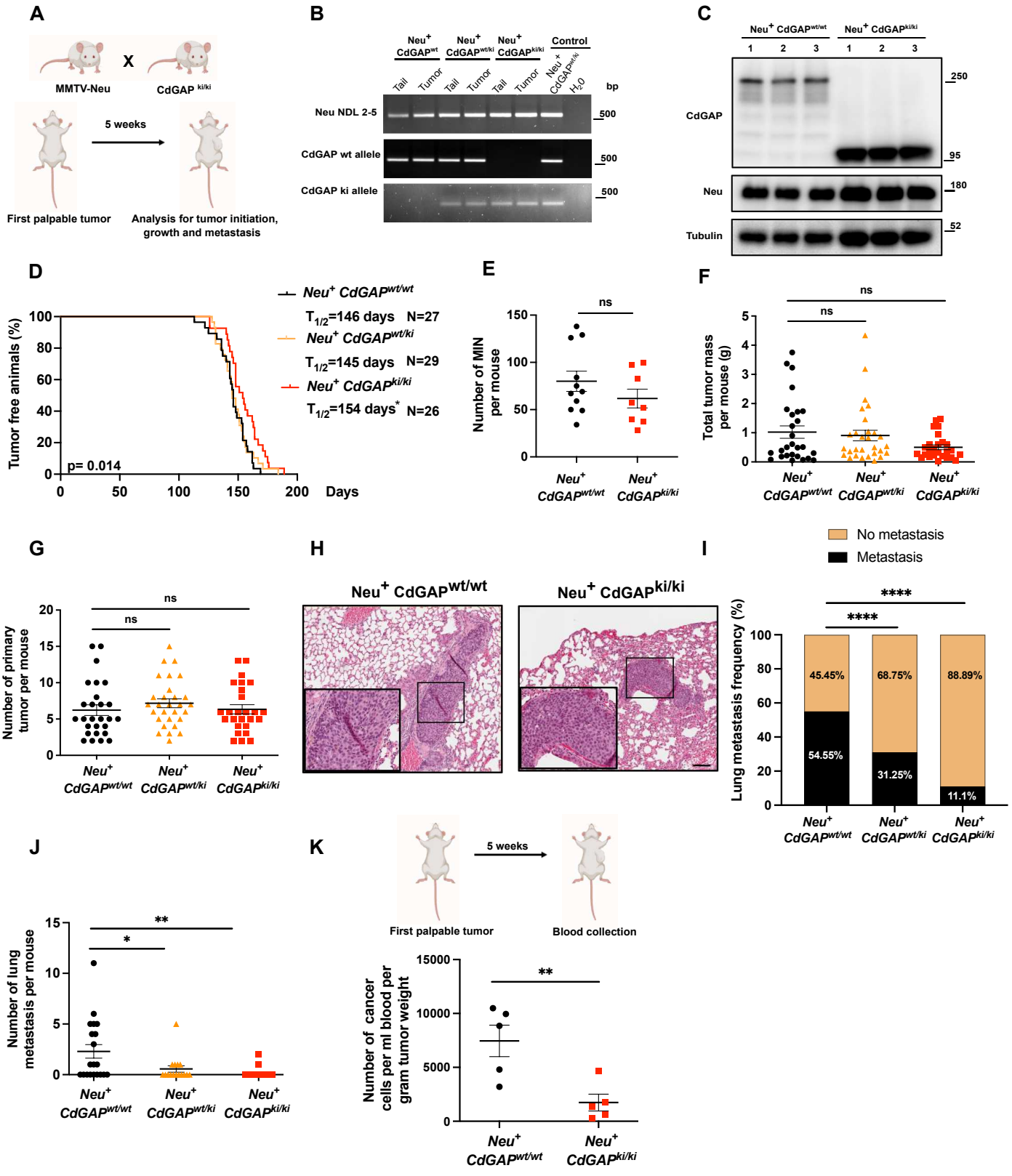

A
MMTV-Neu
X
CdGAP ki/ki
5 weeks
First palpable tumor
Analysis for tumor initiation, growth and metastasis
B
Neu+ CdGAPwt
Neu+ CdGAPwt/ki
Neu+ CdGAPki/ki
Control
Tail
Tumor
Neu NDL 2-5
CdGAP wt allele
CdGAP ki allele
bp
500
C
Neu+ CdGAPwt/wt
Neu+ CdGAPki/ki
CdGAP
Neu
Tubulin
250
95
180
52
D
Tumor free animals (%)
Neu+ CdGAPwt/wt
T1/2=146 days N=27
Neu+ CdGAPwt/ki
T1/2=145 days N=29
Neu+ CdGAPki/ki
T1/2=154 days* N=26
p= 0.014
Days
E
Number of MIN per mouse
ns
F
Total tumor mass per mouse (g)
ns
G
Number of primary tumor per mouse
ns
H
Neu+ CdGAPwt/wt
Neu+ CdGAPki/ki
I
No metastasis
Metastasis
Lung metastasis frequency (%)
****
45.45%
54.55%
68.75%
31.25%
88.89%
11.1%
J
Number of lung metastasis per mouse
**
*
K
5 weeks
First palpable tumor
Blood collection
Number of cancer cells per ml blood per gram tumor weight
**

Figure 2

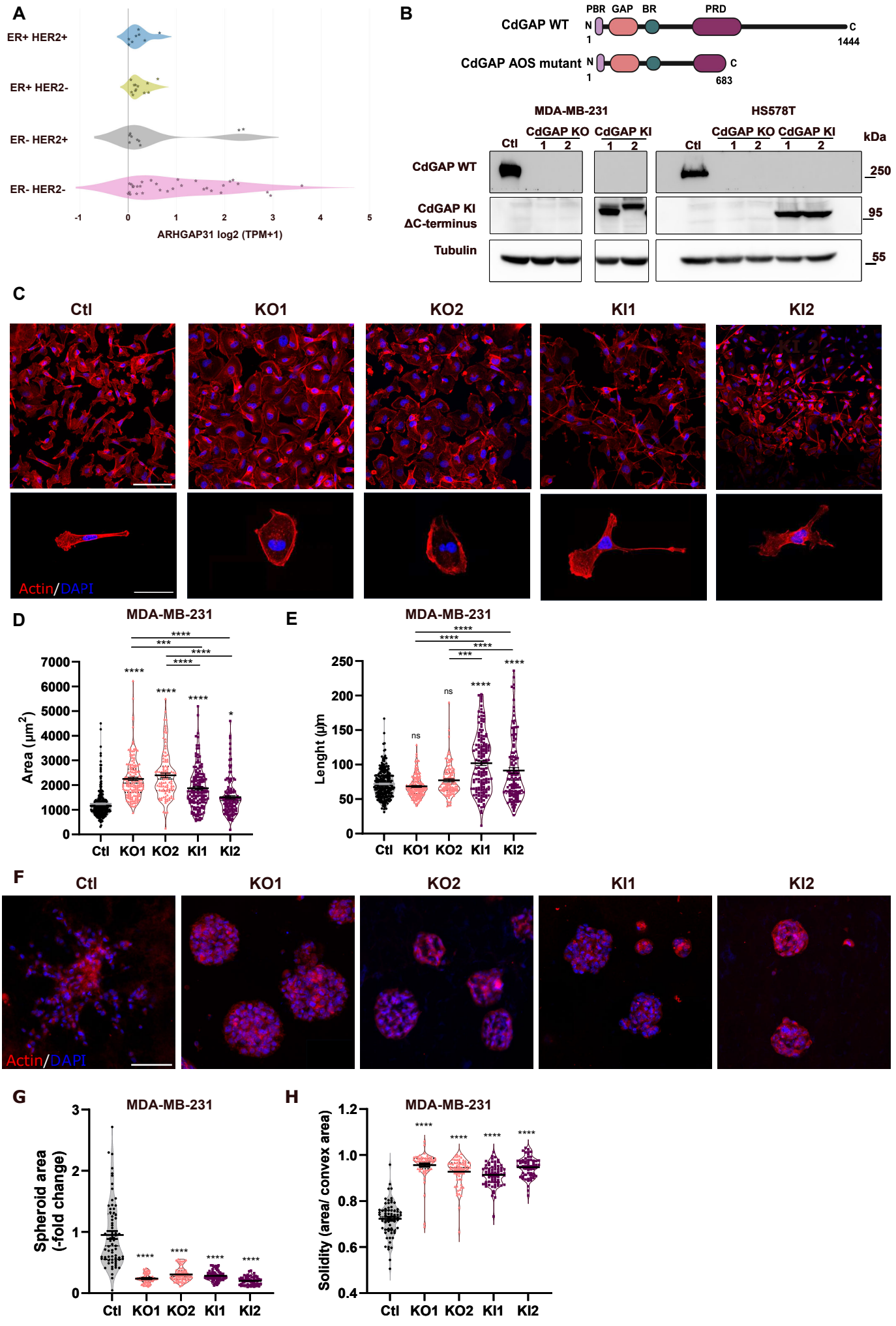

A
ER+ HER2+
ER+ HER2-
ER- HER2+
ER- HER2-
ARHGAP31 log2 (TPM+1)
B
CdGAP WT
PBR GAP BR PRD
CdGAP AOS mutant
MDA-MB-231
HS578T
CdGAP KO
CdGAP KI
Ctl
kDa
CdGAP WT
CdGAP KI ΔC-terminus
Tubulin
250
95
55
C
Ctl
KO1
KO2
KI1
KI2
Actin/DAPI
D
MDA-MB-231
Area (µm²)
E
MDA-MB-231
Lenght (µm)
F
Actin/DAPI
G
MDA-MB-231
Spheroid area (-fold change)
H
MDA-MB-231
Solidity (area/ convex area)

Figure 3

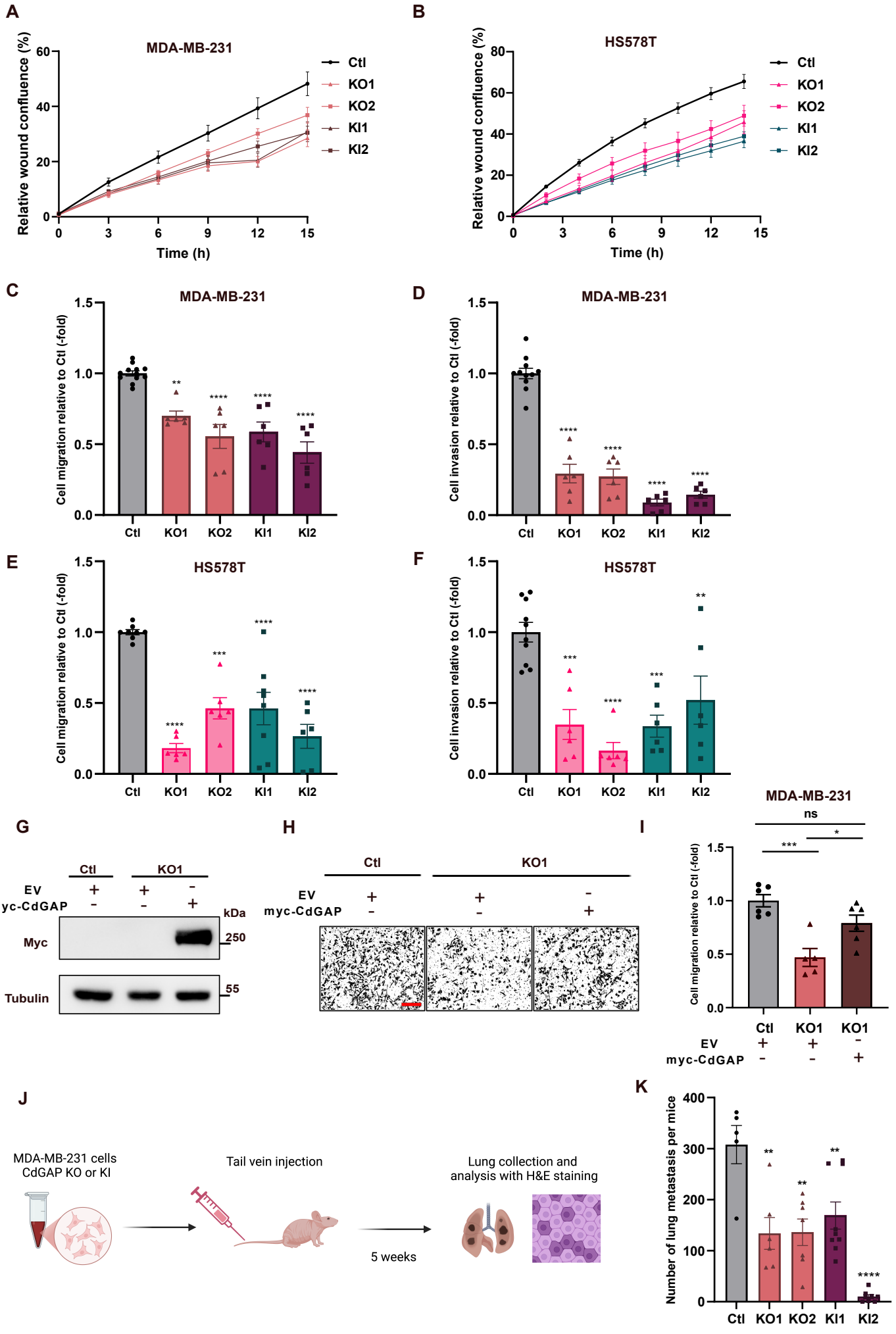

A
MDA-MB-231
Relative wound confluence (%)
Time (h)
Ctl
KO1
KO2
KI1
KI2
B
HS578T
C
MDA-MB-231
Cell migration relative to Ctl (-fold)
D
MDA-MB-231
Cell invasion relative to Ctl (-fold)
E
HS578T
F
HS578T
G
Ctl
KO1
EV
myc-CdGAP
kDa
Myc
250
Tubulin
55
H
I
MDA-MB-231
ns
J
MDA-MB-231 cells
CdGAP KO or KI
Tail vein injection
5 weeks
Lung collection and
analysis with H&E staining
K
Number of lung metastasis per mice

Figure 4

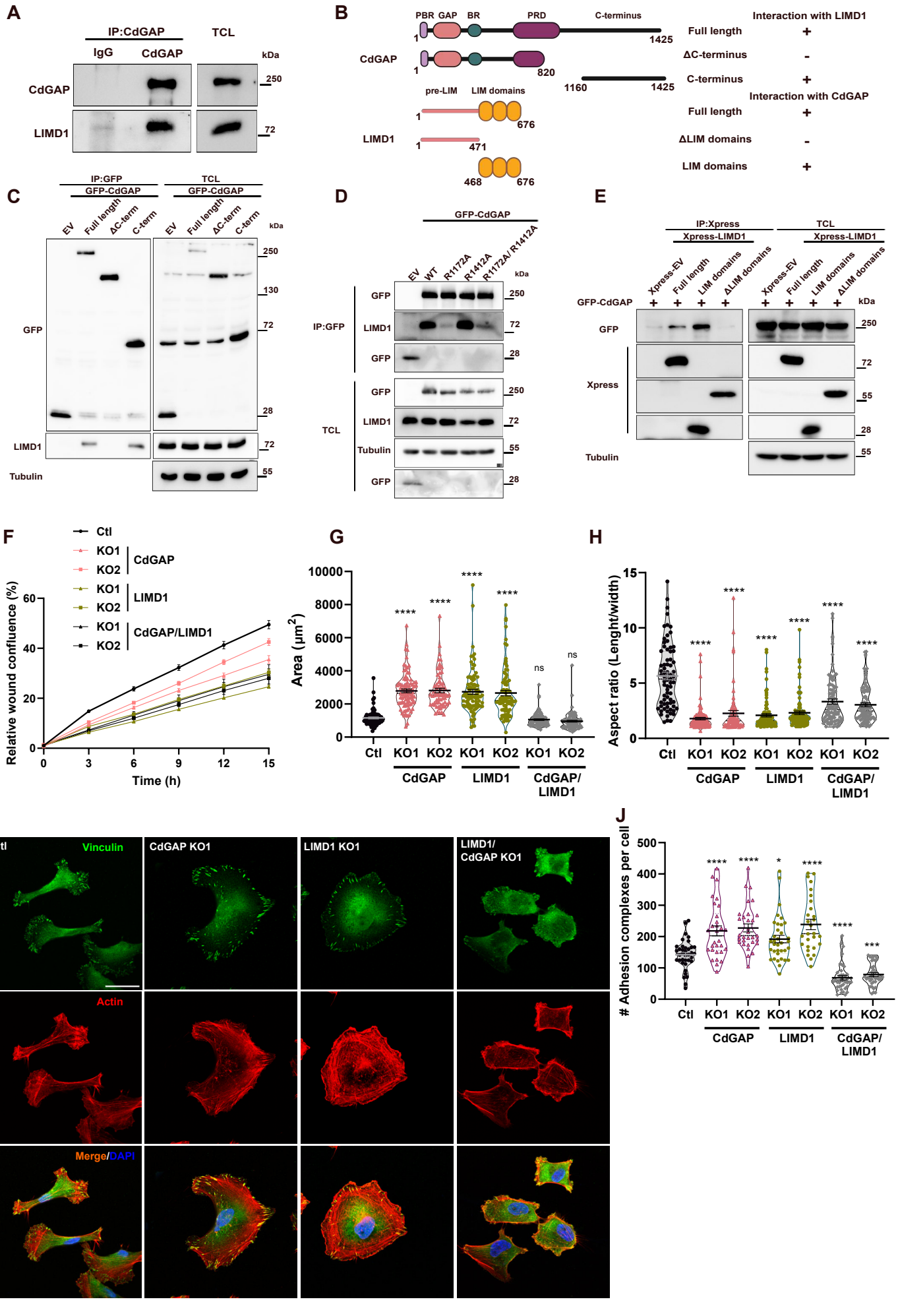

A
IP:CdGAP
TCL
IgG
CdGAP
kDa
CdGAP
LIMD1
250
72
B
PBR GAP BR
PRD
C-terminus
CdGAP
1
820
1160
1425
pre-LIM
LIM domains
LIMD1
471
468
676
Interaction with LIMD1
Full length +
ΔC-terminus -
C-terminus +
Interaction with CdGAP
Full length +
ΔLIM domains -
LIM domains +
C
IP:GFP
TCL
GFP-CdGAP
EV
Full length
ΔC-term
C-term
GFP
LIMD1
Tubulin
250
130
72
28
55
D
GFP-CdGAP
EV
WT
R1172A
R1412A
R1172A/ R1412A
IP:GFP
TCL
GFP
LIMD1
Tubulin
250
72
28
55
E
IP:Xpress
TCL
Xpress-LIMD1
Xpress-EV
Full length
LIM domains
ΔLIM domains
GFP-CdGAP
GFP
Xpress
Tubulin
250
72
55
28
F
Ctl
KO1
KO2
CdGAP
LIMD1
CdGAP/LIMD1
Relative wound confluence (%)
Time (h)
G
Area (μm2)
Ctl
KO1 KO2 KO1 KO2 KO1 KO2
CdGAP
LIMD1
CdGAP/ LIMD1
****
ns
H
Aspect ratio (Lenght/width)
I
Ctl
Vinculin
CdGAP KO1
LIMD1 KO1
LIMD1/ CdGAP KO1
Actin
Merge/DAPI
J
Adhesion complexes per cell
*
***

Figure 5

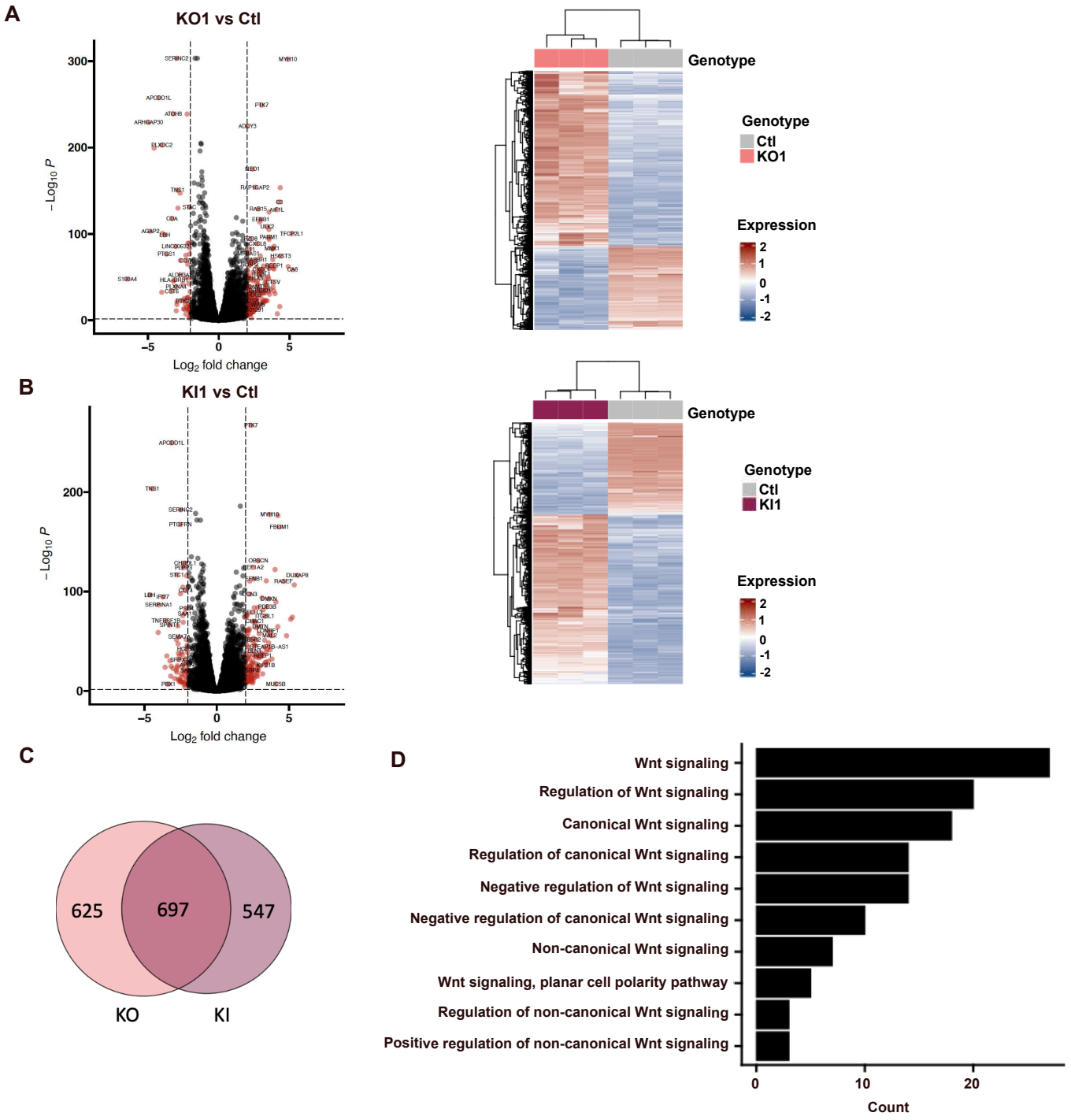

A
KO1 vs Ctl
300
200
100
0
−Log10 P
−5
0
5
Log2 fold change
Genotype
Genotype
Ctl
KO1
Expression
2
1
0
-1
-2
B
KI1 vs Ctl
200
100
0
−Log10 P
−5
0
5
Log2 fold change
Genotype
Genotype
Ctl
KI1
Expression
2
1
0
-1
-2
C
625
697
547
KO
KI
D
Wnt signaling
Regulation of Wnt signaling
Canonical Wnt signaling
Regulation of canonical Wnt signaling
Negative regulation of Wnt signaling
Negative regulation of canonical Wnt signaling
Non-canonical Wnt signaling
Wnt signaling, planar cell polarity pathway
Regulation of non-canonical Wnt signaling
Positive regulation of non-canonical Wnt signaling
0
10
20
Count
E
Genotype
PORCN
TLE3
ZNF703
PLPP3
NDP
NPHP4
LZIC
CTNNBIP1
PRICKLE1
APCDD1L
LRP1
PLEKHA4
ANKRD6
NRARP
PRK7
FDZ8
KREMEN1
TNIK
EDNRA
FZD4
WNT5A
TERT
APC2
SHISA3
DAB2IP
CD24
HIC1
Genotype
Ctl
KI1
KO1
Expression
2
1
0
-1
-2

Figure 6

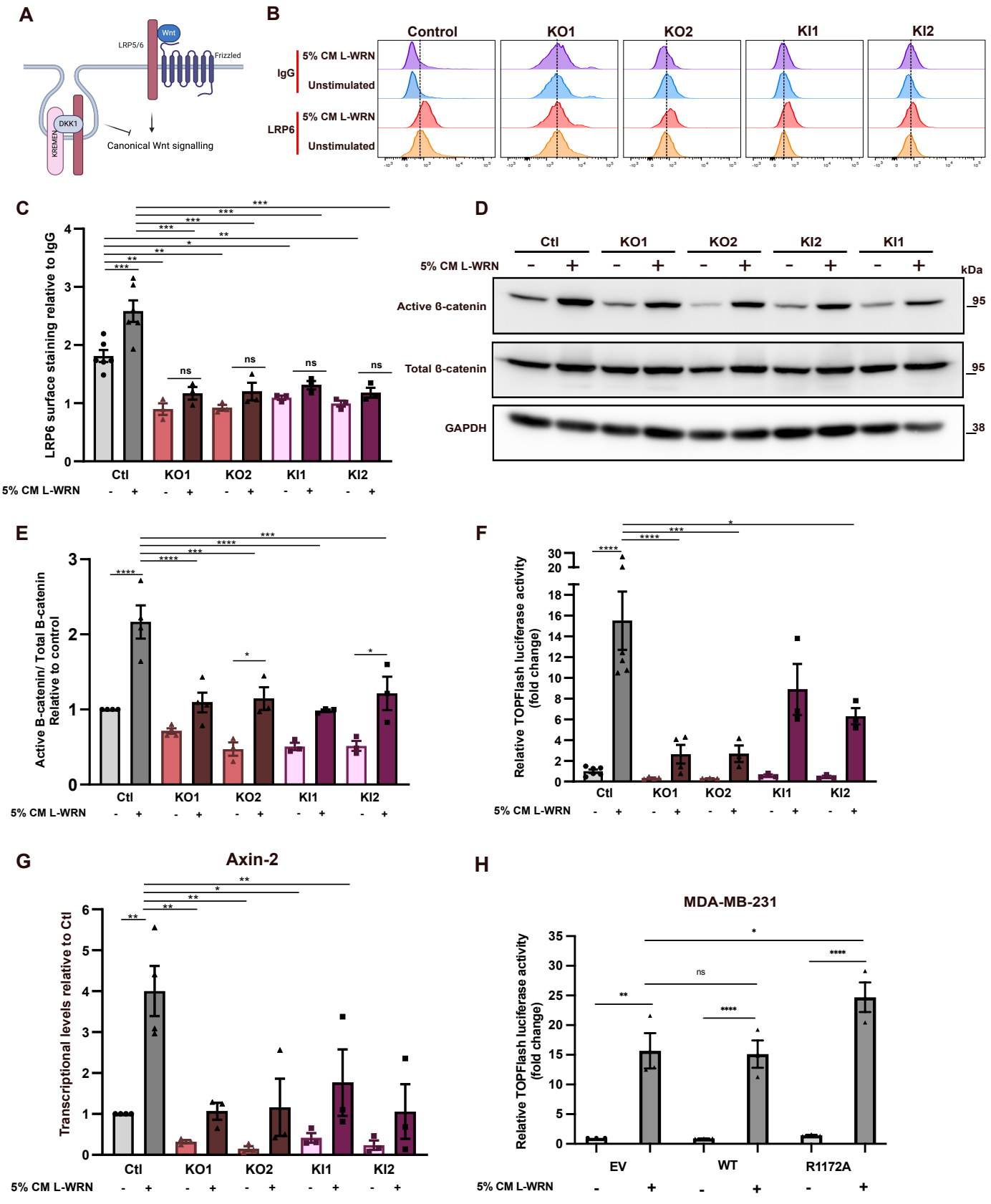

A
Wnt
LRP5/6
Frizzled
DKK1
KREMEN
Canonical Wnt signalling
B
Control
KO1
KO2
KI1
KI2
IgG
5% CM L-WRN
Unstimulated
LRP6
5% CM L-WRN
Unstimulated
C
LRP6 surface staining relative to IgG
Ctl
KO1
KO2
KI1
KI2
5% CM L-WRN
ns
D
Ctl
KO1
KO2
KI2
KI1
5% CM L-WRN
kDa
Active ß-catenin
Total ß-catenin
GAPDH
95
95
38
E
Active B-catenin/ Total B-catenin Relative to control
Ctl
KO1
KO2
KI1
KI2
5% CM L-WRN
F
Relative TOPFlash luciferase activity (fold change)
Ctl
KO1
KO2
KI1
KI2
5% CM L-WRN
G
Axin-2
Transcriptional levels relative to Ctl
Ctl
KO1
KO2
KI1
KI2
5% CM L-WRN
H
MDA-MB-231
Relative TOPFlash luciferase activity (fold change)
ns
EV
WT
R1172A
5% CM L-WRN

Figure 7

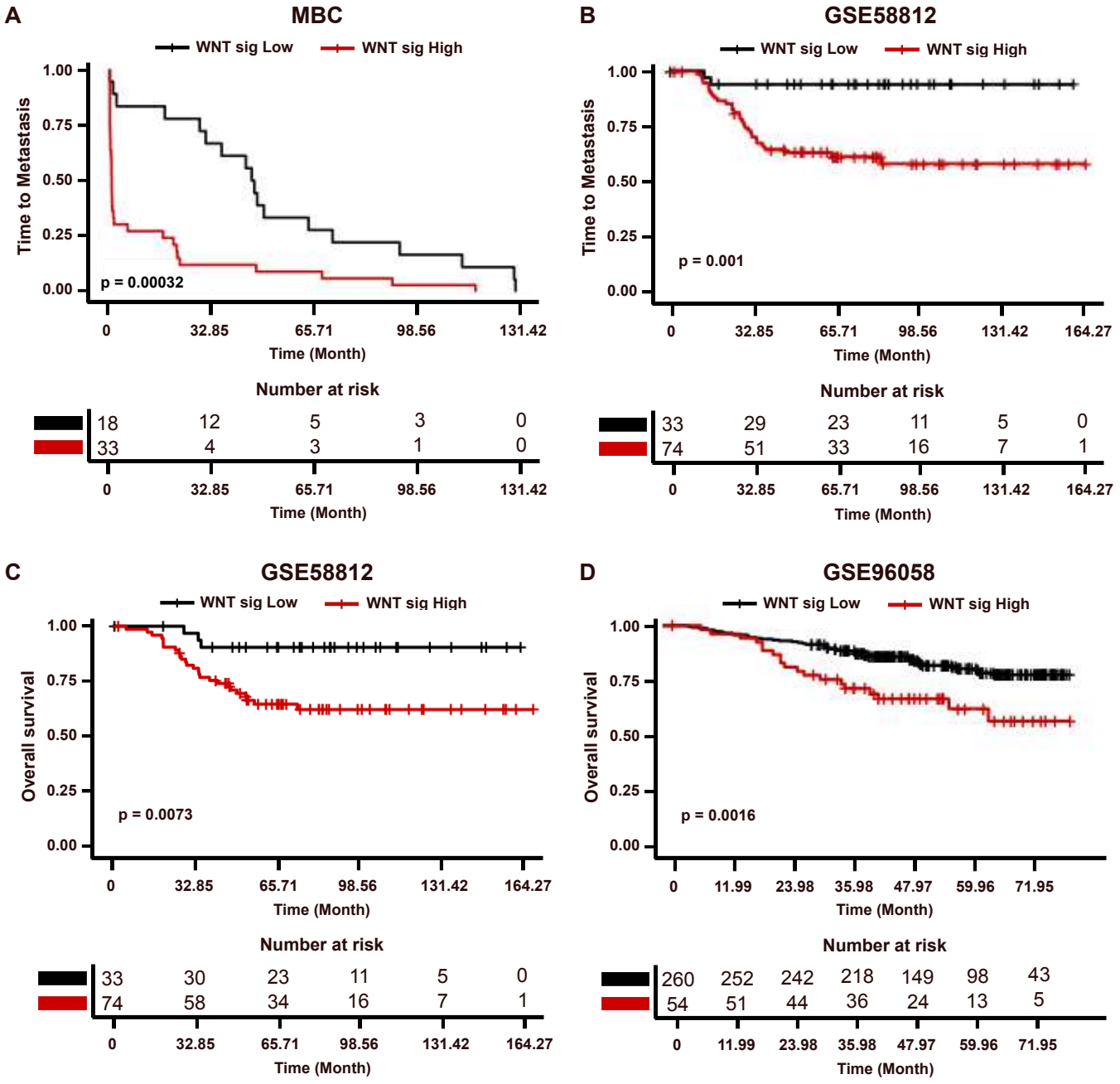
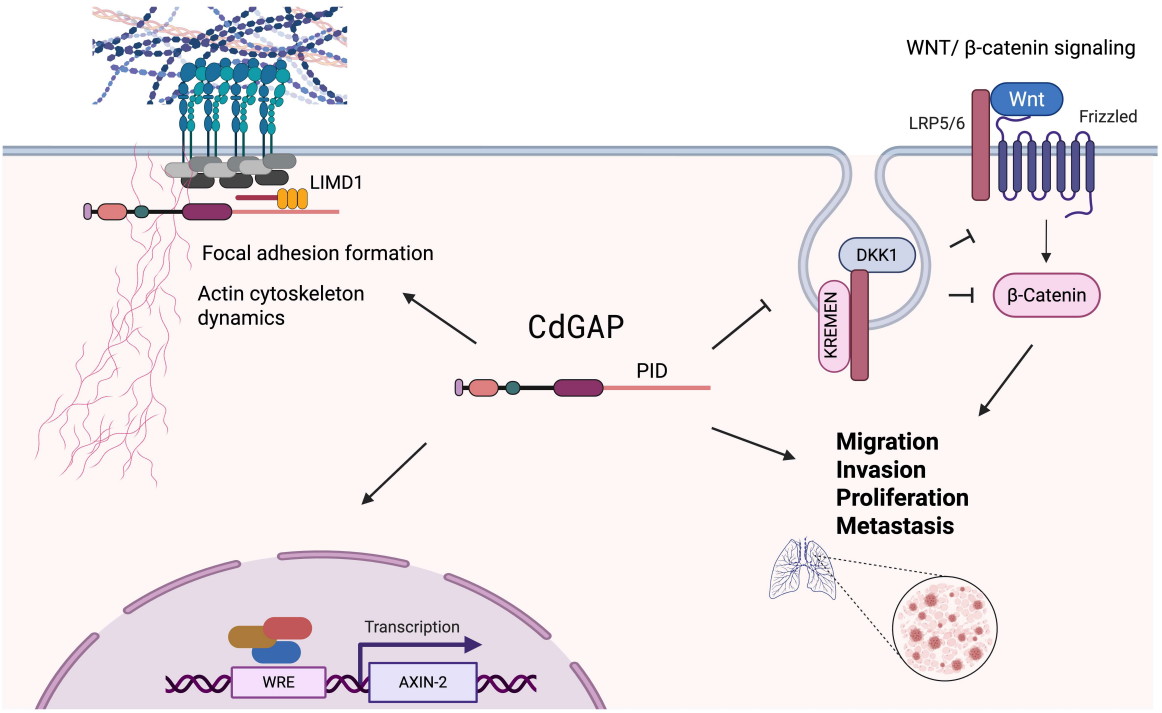

A
MBC
WNT sig Low
WNT sig High
Time to Metastasis
1.00
0.75
0.50
0.25
0.00
p = 0.00032
0
32.85
65.71
98.56
131.42
Time (Month)
Number at risk
18 12 5 3 0
33 4 3 1 0
B
GSE58812
WNT sig Low
WNT sig High
Time to Metastasis
p = 0.001
0
32.85
65.71
98.56
131.42
164.27
Time (Month)
Number at risk
33 29 23 11 5 0
74 51 33 16 7 1
C
GSE58812
WNT sig Low
WNT sig High
Overall survival
p = 0.0073
0
32.85
65.71
98.56
131.42
164.27
Time (Month)
Number at risk
33 30 23 11 5 0
74 58 34 16 7 1
D
GSE96058
WNT sig Low
WNT sig High
Overall survival
p = 0.0016
0
11.99
23.98
35.98
47.97
59.96
71.95
Time (Month)
Number at risk
260 252 242 218 149 98 43
54 51 44 36 24 13 5

Figure 8


WNT/ β-catenin signaling
Wnt
LRP5/6
Frizzled
LIMD1
Focal adhesion formation
Actin cytoskeleton dynamics
CdGAP
PID
DKK1
KREMEN
β-Catenin
Migration
Invasion
Proliferation
Metastasis
Transcription
WRE
AXIN-2

Supplementary Files

This is a list of supplementary files associated with this preprint. Click to download.

- FIGURES1.pdf
- FIGURES2.pdf
- FIGURES3red.pdf
- FIGURES4red.pdf
- FIGURES5.pdf
- FIGURES6red.pdf
- FIGURES7red.pdf
- FIGURES8.pdf
- FIGURES9.pdf
- SupplementaryFigurelegends190526copy.pdf
- TABLE5RNAseqfinal.xlsx
- TABLE6WNTStatisticalanalysis.xlsx
- Table1.xlsx
- Table2.xlsx
- Table3.xlsx
- Table4.xlsx